A detailed spectral analysis of the 10 keV feature in accreting X-ray pulsars

Dimitrios K. Maniadakis

Bachelor Thesis

Department of Physics, University of Crete

Supervisor: Pablo Reig

Contents

Chapter 1: Introduction

1.1 X-ray binary systems

X-ray binary systems are binary stars consisting of a star and a compact object. They are luminous mostly in X-ray radiation that is produced via accretion, that is when the matter falls from the star or donor onto the compact object or accretor due to the gravitational potential of the latter. Since they are luminous not only in the X-ray region, but in the optical too, it can be concluded that nuclear burning is still occurring in the star's core ("optical companion") (P. Reig 2011)

1.2 Classification

These systems can be divided in to three main classes, where the compact object is a White dwarf, a Black hole or a Neutron star. In the last two cases, they can be further divided in to low mass X-ray binaries (LMXBs) if the type of the donor is A or later and high mass X-ray binaries (HMXBs), if the donor is O or B. (fig. 1.1).

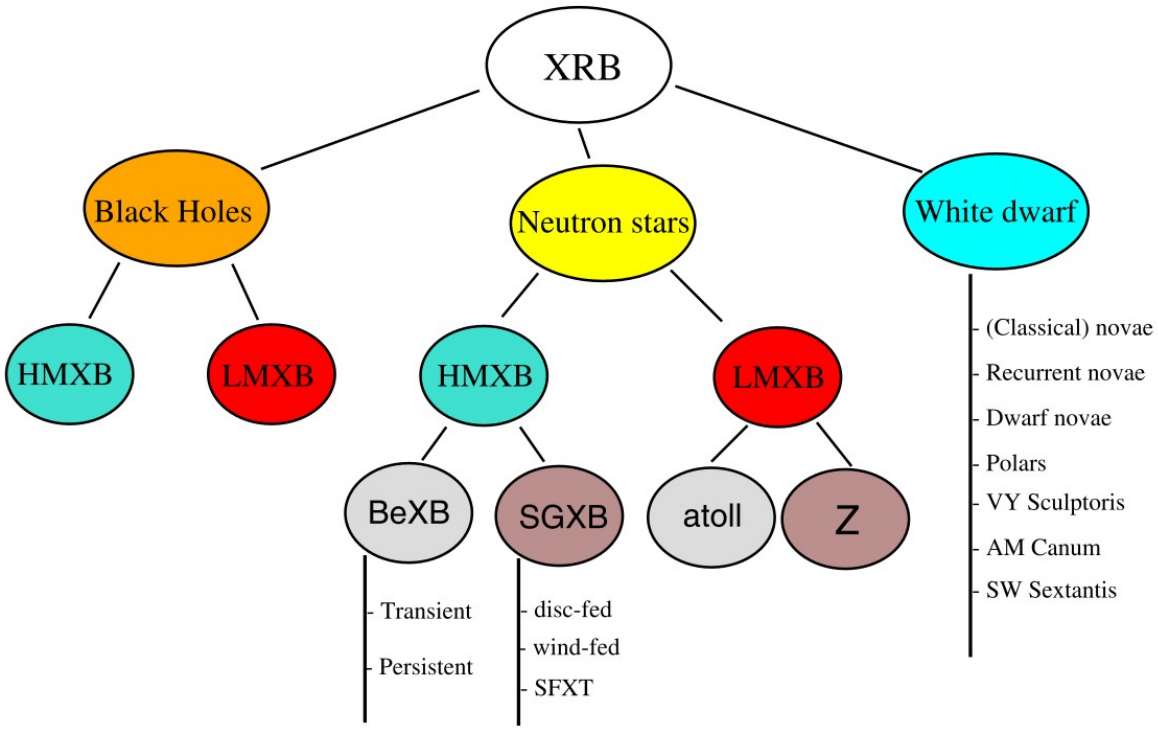

Figure 1.1: Classification of X-ray binaries (P. Reig 2011)

1.2.1 Low mass X-ray binaries

Low mass X-ray binaries consist of a star with a type A or later, or in some cases a white dwarf, and a compact object which is a neutron star or a black hole. They radiate mainly on the soft X-ray spectra. They do not have a strong stellar wind and thus the mass transfer from the donor to the compact object is usually done via Roche lobe overflow, where an accretion disk is created (M.C. Ramadevi 2007). More precisely, Roche lobe overflow occurs when a star fills it's own Roche lobe, the area where all matter is gravitational bound to the star. Then, material flows to the star's companion via the first Lagrangian point, one of the five in which a small object will maintain its position, relative to the other two bodies (Biswajit Paul and Sachindra Naik 2011). Most of the radiation produced is in X-rays and less than one percent is in the visual spectrum.

1.2.2 High mass X-ray binaries

High mass X-ray binaries consist of a star with a type O or B and a compact object which is a neutron star or a black hole. In these systems, the donor dominates the optical and IR spectrum, as the compact object dominates in the X-ray spectrum. The X-ray radiation can be produced with three different kinds of mass transfer. The most usual is when the compact object is wind fed: the X-rays are produced as the stellar wind falls in to the compact object. Secondly, like in the LMXBs, Roche lobe overflow can occur resulting in an accretion disk. Thirdly, there can be accretion from the circumstellar disk of the star, if there is one, causing x-ray outbursts. In the case of high mass/neutron star binaries, we can further divide in to two subcategories: Be/X-ray binaries (BeXBs) and Super giant X-ray binaries (SGXBs) (Biswajit Paul and Sachindra Naik 2011).

Super giant X-ray binaries or SGXBs consists of a type I or II luminosity class star, while the compact object is a neutron star. They emit a strong stellar wind, removing 10^{-6} - 10^{-8} M_O per year, with high velocities (~2000 km s^{-1}). The X-ray emission is persistent and very bright, and hence these systems were the first to be discovered. A neutron star that has a close orbit, will attract a part of the wind and will produce X-rays. If the star has exceeded its Roche lobe, then there can be accretion via Roche lobe overflow. So far, there have been dozens of wind fed SGXBs but only three disc fed. (P. Reig 2011).

1.3 Be/X-ray binaries

1.3.1 Be stars

In order to talk about Be/X-ray binaries, we first have to discuss the nature of Be stars.
The classical definition is the following (G. W Collins 1987):

"A non-supergiant B star whose spectrum has or had at some time, one or more Balmer lines in emission"

This definition is problematic, since every B star with some sort of circumstellar material with densities above 10^{-13} gr/cm^3 will form Balmer line emission around the star (Thomas Rivinius, Alex C. Carciofi, Christophe Martayan 2013) but on the case of a Be star, the emission originates from a circumstellar disk of material that surrounds it.

More specifically, it is an outward gaseous Keplerian disk that is fed from the mass the star ejects. The formation of these disks is still unclear to the astronomers. It is known that Be stars rotate rapidly but most of them do not rotate critically, in order for material to go on a Keplerian orbit and feed the disk, so there must be another mechanism. Many theories have been proposed over the years, but none of them offer a complete explanation.

From an observation point, the spectral energy distribution results from photospheric emission, disk emission of reprocessed radiation and disk absorption. The main characteristics are the excess IR radiation and the Balmer lines in emission as mentioned above. Both originates from the disk: IR is produced from the heat of the disk, and Balmer lines from the reprocessed radiation (Thomas Rivinius, Alex C. Carciofi, Christophe Martayan 2013).

1.3.2 Be/X-Ray Binaries

Be X-ray Binaries (BeXBs) are HMXBs that have a Be star as an optical companion. They represent the largest group of HMXBs (K. Hayasaki and A. T. Okazaki 2004). All the BeXBs that had been observed before 2014 had a neutron star as the compact object of the system. In 2014, a BeXB with a black hole as the compact object was observed (MWC 656) (Casares et al. 2014).

The neutron star, during periastron passage, gets close to the disk and sometimes causes a major disruption. The disk material is accreted to the neutron star due to the gravity of the latter and the free fall kinetic energy is converted into thermal energy that leads to X-ray emission (P. Reig 2011). The material is directed to the magnetic poles and funneled into accretion columns when it finally reaches the surface. The accretion column is where most of the X-ray radiation is produced. In most cases, the magnetic and rotation axes are not aligned. As a result, the X-ray emission appears to pulsate with the spin period of the neutron star (S. Rosswog and M. Bruggen 2007). The pulsations of a BeXB can be a few seconds (4U 0115+634) or even a few tens of minutes (LS I +61 235) (P. Reig 2011).

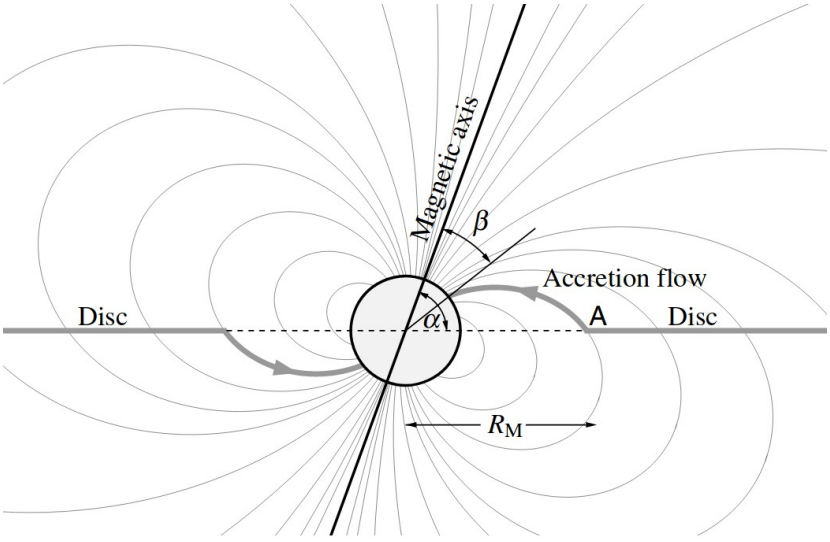

Figure 1.2: Accretion of a magnetized neutron star from a disk (Frank et al. 1992, Fig. 6.4).

1.3.3 X-ray properties

There are two kinds of BeXB sources: persistent and transient. Reig and Roche (1999) introduced the subclass of persistent sources. Until then, only one (X-Per) was known, but there have been

multiple persistent sources detected since then. The key differences between the two types of sources are the following:

Persistent

The X-ray emission is persistent, with low luminosity ($L_{2-20\ keV} \sim 10^{34-35}$ erg s^{-1}). There are small unpredicted increases in intensity by less than an order of magnitude. The iron line at ~6.4 keV is weak, indicating a small amount of material in the vicinity of the pulsar. The pulsar itself has a big rotation period ($P_{spin} \geq 200$ seconds) (P. Reig 2011).

In these systems, the pulsar does not get close enough to the Be star and therefore it never enters the denser inner regions of the circumstellar disc (Reig and Roshe 1999). The orbital period is big ($P \geq 200$ days) and the eccentricity is small (e ~ 0.1-0.2) (P. Reig 2011).

Transient

The vast majority of BeXBs are transient sources. The X-ray emission in characterized by small (type I) and big (type II) outbursts.

Type I outbursts are regular and periodic (or quasiperiodic). They happen on every periastron passage of the pulsar. They are short lived and cover ~0.2-0.3 of the orbital period. The X-ray flux is increased by about one order of magnitude, while the luminosity can reach up to ~10^{36-37} erg s^{-1} (P. Reig 2011).

Type II outbursts are unpredictable. They can last up to several times the orbital period. The X-ray flux can be increased ~10^{3-4} times, reaching the Eddington limit of the neutron star and becoming the brightest object in the X-ray sky. Many believe that an accretion disk is formed during the outburst (Wilson et al. 2008). This argument can be supported by the discovery of quasi-periodic oscillations in some systems as well as the spin-up rates observed during an outburst (P. Reig 2011). Most times, as a result of the outburst, a big disturbance on the structure of the disk can happen, even the disappearance of the disk. But type I outbursts have been observed that had no effect on the disk.

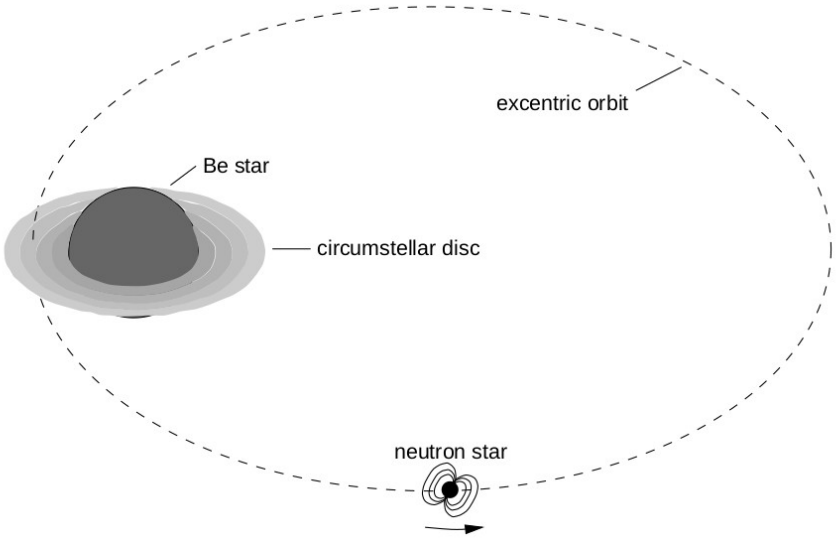

Figure 1.3: Orbit of a neutron star in a Transient X-ray binary (Kretschmar, 1996, Fig. 2.6).

1.4 Cyclotron lines

Highly magnetized accreting pulsars show line-like features in their X-ray spectra, mostly in absorption, in the 10-100 keV energy range. These features are called cyclotron resonant scattering features (CRSFs) or cyclotron lines. They originate from the resonant scattering of photons on electrons, on the hot magnetized plasma close to the magnetic moles of the accreting pulsar. The electrons assume discrete energies, with respect to their movement perpendicular to the magnetic field, the Landau levels. The centroid line energies are given by the following relation:

$$E_{cyc} = \frac{n}{1+z} \cdot \frac{\hbar e B}{m_e c} \approx \frac{n}{1+z} \cdot 11.6\,[keV] \times B_{12}$$

where B_{12} is the magnetic field strength in units of 10^{12} Gauss, z the gravitational redshift and n the number of the Landau level (R. Staubert et al. 2018).

1.5 X-ray reflection

The Reflection spectrum from X-ray accreting sources is produced from the irradiation of the accretion flow. It mainly consists of backscattered radiation, fluorescence, recombination and other emissions (A.C. Fabian and R.R. Ross 2010).

Cold reflection

If the irradiation is weak and the gas dense, there is cold reflection. The albedo on cold reflection depends on electron scattering which dominates the spectrum on energies above 20 keV and photoelectric absorption which dominates at lower energies (Basko et al. 1974). Compton scattering leads to a hump known as “Compton hump” at the energy range of 20-40 keV (A.C. Fabian and R.R. Ross 2010).

The X-ray reflection in the innermost regions around black holes was computed by Lightman and White (1988) by using a Green’s function approach, leading to the creation of the PEXRAV model in XSPEC by Magdziarz and Zdziarski (1995). The fluorescence line of Iron was not included in this computation (A.C. Fabian and R.R. Ross 2010).

Iron fluorescence line

The cold reflection spectrum include the fluorescence emission lines. Fluorescence excitation occurs when a gas with low ionization is illuminated by X-ray radiation. In the case of X-ray binaries, the accretion produces the X-ray photons that illuminates the circumstellar material, either the wind or the accretion disk (J.M. Torrejon et al. 2010).

On the case of hard X-rays, the photons are mostly absorbed by elements with high atomic numbers so the emission is strong for iron (A.C. Fabian and R.R. Ross 2010). The iron present, absorb a significant amount of continuum photons with energies equal or higher than the K edge (~7.1 keV). The K-shell electrons leave a vacancy that is occupied by the L-shell or M-shell electrons and thus the fluorescence emission lines Kα (6.4 keV) and Kβ (7.1 keV) are produced. The structure of the line consists of two components, one broad (FWHM ~ keV) and one narrow (FWHM ~ eV)

component (J.M. Torrejon et al. 2010). The iron fluorescence line is correlated with the Compton hump.

The fluorescence photons can louse energy due to Compton scattering, if the circumstellar material is Compton thick and they further travel through it before reaching the interstellar medium. That is called “Compton shoulder” (J.M. Torrejon et al. 2010).

1.6 The 10 keV feature

A peculiar feature around ~10 keV was first reported by Coburn in 2002. It was a “bump”, in the energy range of 8-12 keV. The feature was also evident in earlier work, on 4U 1538-52, 4U 1907+09 and V0331+53 (Mihara 1995), but also on Cen X-3 (Santangelo et al. 1998). Since then, it has been reported multiple times for many X-ray sources. In the case of BeXBs, the feature has been reported only for transient sources. The feature has been detected in observations with RXTE, BeppoSAX, Ginga and Suzaku.

It can be mistaken for a CRSF, but Coburn (2002) argued that since the bump is consistent at or near 10 keV, it cannot be a magnetic effect. It is also evident in sources that do not exhibit cyclotron lines. Despite of that, Farinelli et al. 2016 constructed a new model for the X-ray continuum of magnetized accreting pulsars, which included the 10-keV feature as a cyclotron emission. Until today, the origin of the 10 keV feature remains unknown.

1.7 Aim of the project

The goal of this project was to test if the residuals at 8-12 keV are gone if a broad gaussian in emission is concluded to the model at 12-18 keV, and to provide a physical explanation about the origin of the 10-keV feature, testing whether or not it can be due to reflection on cold material around the pulsar. All 12 systems we chose for this project are transient Be/X-ray binaries and the data comes from Type II outbursts, since the feature has been detected in such events. We used three models: a simple power law with high energy cut-off, a phenomenological model using broad Gaussian in emission and a physical reflection model.

Chapter 2: Observations

We used the data obtained from the Rossi X-ray Timing Explorer (RXTE), for twelve transient Be/ X-ray binaries. For each system, we took the spectra for three different luminosities from the same outburst. We, then, fitted the data, assuming a 0.5% systematic error, with three different models (see Section 2.2): an absorbed power law with a cut-off energy and two models, a physical and a phenomenological model. The first one contains one extra component, a gaussian component, and the other represent reflection from cold material in the vicinity of the compact object. We performed an F-test to compare those two models with respect to the simple model.

2.1 X-ray observations: The Rossi X-ray Timing Explorer

The Rossi X-ray Timing Explorer (RXTE) was launched in December 1995 for the purpose of exploring the variability of X-ray sources. It was in orbit around the Earth for 16 years, until January 2012. The orbital period was 90 minutes, at an altitude of 580 km with an inclination of 23 degrees. The RXTE could observe the energy range between 2 to 250 keV, on time scales from microseconds to months.

The instruments

RXTE hosted three instruments: the All-Sky Monitor (ASM), the Proportional Counter Array (PCA) and the High Energy X-ray Timing Experiment (HEXTE).

The All-Sky Monitor (ASM**)** was able to scan ~80% of the sky every orbit, monitoring the X-ray sky at time scales of at least 90 minutes, to detect outbursts from transient sources (Levine et al. 1996). The ASM consisted of three Scanning Shadow Cameras (SSCs). The energy range that the ASM could observe was 2-10 keV and its sensitivity was 30 mCrab.

The High Energy X-ray Timing Experiment (HEXTE) could detect energies between 15 and 250 keV (Rothschild et al. 1998). It consisted of two clusters of detectors. The collecting area of each cluster was 800 cm^2. It's sensitivity was 1 Crab and the energy resolution was 15% at 60 keV.

The Proportional Counter Array (PCA) was able to take observations on the energy range of 2-60 keV with the accuracy of one microsecond. It was a photo counting instrument and not an imaging one. It consisted of 5 large proportional counter units (PCU). Each of them had an effective area of 1300 cm^2. Behind the collimator two mylar windows define a gas volume of Propane, at pressure of about 802 torr and 22^o C. Behind the second window was the main volume that was filled with a Xenon (90%) - Methane (10%) mixture on a pressure of about 840 torr (Jahoda et al. 2006). The detection process was the following: The X-ray photon induces an electron current that goes towards the anodes within the gas chamber, where the Xenon-Methane mixture is located. The chamber had three layers with different anode chains, with a voltage of about 2000 volts. The accelerated electrons ionize the gas molecules, while they are heading to the anodes, producing more electrons. The current's intensity is proportional to the X-ray photon's energy. The energy resolution of the PCU was 18% at 6 keV. It's sensitivity was 0.1 mCrab (https://heasarc.gsfc.nasa.gov/docs/xte/appendix_f.html).

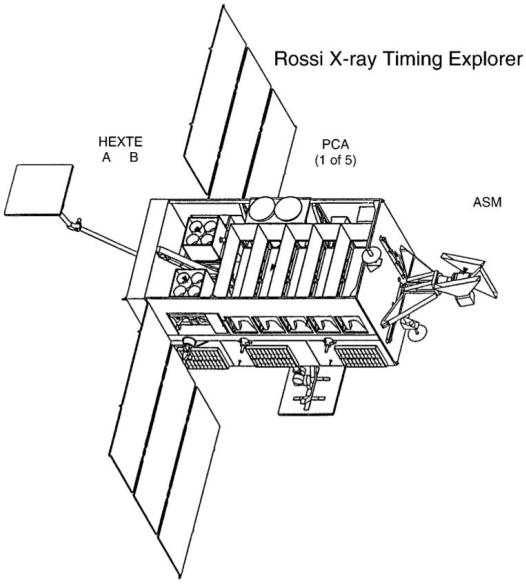

Figure 2.1: the RXTE spacecraft (Rothschild et al. 1998)

2.2 Spectral Analysis

2.2.1 XSPEC

The program used for the spectral analysis was XSPEC version 12.10.1.

XSPEC is a command driven, detector-independent X-ray spectral-fitting program (*https://heasarc.gsfc.nasa.gov/xanadu/xspec/manual/XspecManual.html*). The first version was written in 1983 at the Institute of Astronomy on Cambridge, under VAX/VMS by Rick Shafer. It was designed to fit the data from the European Space Agency - European X-ray Observatory Satellite (ESA EXOSAT) X-ray observatory, which was launched the same year. Rick Shafer later enhanced the VAX/VMS version when he joined the EXOSAT group, while Keith Arnaud ported XSPEC to a Sun/UNIX operating system. For several years these two versions were separate until there was recovered a single version: the XSPECv6.

2.2.2 The Basics of Spectral Fitting

The observed spectrum C(I) is related to the actual spectrum of the source f(E) by the following relation:

$$C(I)=\int f(E)\,R(I,E)\,dE$$

where R(I,E) is the response of the instrument. This relation is not invertible, since the equation is very unstable under small changes of C(I). Since we can not take the actual spectrum f(E), the alternative is to find a model spectrum $f_b(E)$ with parameters that can fit the data. The parameters are varied and a predicted count spectrum then is calculated and compared to the observed data. A fit statistic is used for the comparison of the actual spectrum and the model, to determine whether the model fits the data or not.

The most common fit statistic is χ^2 and is defined by the following relation:

$$\chi^2=\frac{\sum (C(I)-C_p(I))^2}{(\sigma(I))^2}$$

where σ(I) is the error for channel I and is usually estimated by $\sqrt{C(I)}$. The goodness of the fit depends on the value of χ^2. As a general rule, the fit is considered good when $\chi^2 \sim \nu$, where ν is the degrees of freedom of the model. The degrees of freedom are defined as the number of channels minus the number of model parameters. If the reduced χ^2 is equal to χ^2 over ν, we want it to be as close to 1 as possible. If it takes values lower than 1, then it's possible that the errors have been overestimated.

2.2.3 General, Bump and Reflection models

In our project, we used data from Standard-2 observing mode of PCA with 129 channels between 2–60 keV, for twelve Be/X-ray binary systems, each of them on an outburst. We used the channels 4-50 for our analysis (energy band: ~3-22 keV) since below 4 keV PCA is not very sensitive and above 22 keV the spectrum becomes background dominated. The model components we used to fit the data are the following:

First of all, the photoelectric absorption of the interstellar medium needs to be contained in our model. The component used for this purpose is the **PHABS** model, which uses cross-sections from the *xsect* (Balucinska-Church & McCammon 1992) command:

$$M(E)=\exp[-n_h\sigma(E)]$$

where σ(E) is the photoelectric cross-section (not including Thomson scattering). The free parameter is the column density n_h in cm^{-2}. Since the photoelectric absorption mainly affects energies lower than 3 keV, we do not necessarily expect the parameters to take logical values.
For the continuum of the source, we need a power law with high energy exponential cut-off . The model we used is the **CUTOFFPL** model:

$$A(E)=KE^{-\Gamma}\exp(\frac{-E}{E_{cut}})$$

The free parameters on this model are the photon index Γ (power law index), the cut-off energy E_{cut} (exponential roll-off on higher energies) and the normalization K in photons keV^{-1} cm^{-2} s^{-1}.

We also expect a fluorescent iron line emission at ~6.4 keV. For this purpose, we will use a simple Gaussian line profile, which can be achieved with the **GAUSS** model:

$$A(E)=K\frac{1}{\sigma\sqrt{2\pi}}\exp[\frac{-(E-E_l)^2}{2\sigma^2}]$$

The free parameters on this model are the E_l which is the energy of the line in keV, the line width σ in keV and the normalization K in photons keV^{-1} cm^{-2} s^{-1}.

For the case of the existence of a cyclotron line, we can use the **GABS** model:

$$M(E)=\exp\left(\frac{-\tau}{\sqrt{2\pi}}\right)\exp\left(-0.5\left(\frac{E-E_g}{\sigma}\right)^2\right)$$

The free parameters on this model are the energy of the line in keV E_g, the line width σ in keV, and the line depth τ.

To describe reflection, we will use the **PEXRAV** model (Magdziarz & Zdziarski 1995). It calculates the spectrum from an approximation of Green's function for the Compton reflection of X-rays by cold electrons. It's a power law with a high energy exponential cut-off, with a reflection component. Its parameters are:

1. Γ : power law photon index
2. E_c : cut-off energy
3. rel_{ref} : reflection scaling factor (reflection if <0)
4. z : redshift
5. Abundance of elements heavier that He, relative to solar abundances
6. Iron abundance relative to solar abundances
7. Cosine of inclination angle

With these components, we will construct three different models which we will use to fit the data:

- We will call the restricted model, **General model.** It's the one with the fewer parameters. It does not contain any component to fit the 10 keV feature. Its structure is the following:

$$M_{General}=PHABS\times(CUTOFFPL+GAUSS)$$

- We will call the phenomenological model, the **Bump model.** It's the same as the General model, but a broad Gaussian is included at the energy range of 12-18 keV.

$$M_{Bump}=PHABS\times(CUTOFFPL+GAUSS+GAUSS)$$

- We will call the physical model, the **Reflection model.** The input is the same as the General model, but PEXRAV is used as the reflection component. The photon index and the cut-off energy of the latter are fixed to the values of CUTOFFPL.

$$M_{Reflection}=PHABS\times(CUTOFFPL+PEXRAV+GAUSS)$$

  In this model, we kept the normalization of PEXRAV fixed and equal to 1. The cut-off energy and the photon index of PEXRAV were kept fixed to the values of CUTOFFPL. The only parameter that was left free was the reflection scaling factor.

2.3 Data from RXTE

We used the data obtained from the standard mode 2 of PCA. The following table shows the observation ID, the Modified Julian Date and the calculated flux from each model, for each observation.

Table 2.1: Obs-Id, MJD, fluxes (erg cm^{-2} s^{-1}) for each observation.

System	Obs-Id	MJD	Flux General model	Flux Bump model	Flux Reflection model
2S 1417-624	94032-02-05-01	55162.081	$5.86 \cdot 10^{-9}$	$5.73 \cdot 10^{-9}$	$4.93 \cdot 10^{-9}$
	94444-01-03-01	55186.018	$2.60 \cdot 10^{-9}$	$2.60 \cdot 10^{-9}$	$2.57 \cdot 10^{-9}$
	94444-01-04-01	55195.215	$1.84 \cdot 10^{-9}$	$2.62 \cdot 10^{-9}$	$2.62 \cdot 10^{-9}$
4U 1901+03	70096-01-03-04	52689.545	$8.75 \cdot 10^{-9}$	$8.12 \cdot 10^{-9}$	$8.63 \cdot 10^{-9}$
	70096-01-16-01	52780.504	$3.91 \cdot 10^{-9}$	$3.47 \cdot 10^{9}$	$3.43 \cdot 10^{-9}$
	70096-01-21-00	52811.542	$1.99 \cdot 10^{-9}$	$1.62 \cdot 10^{-9}$	$1.41 \cdot 10^{-9}$
1A 1118-61	94032-04-02-09	54845.686	$1.21 \cdot 10^{-8}$	$1.13 \cdot 10^{-8}$	$1.15 \cdot 10^{-8}$
	94032-04-03-05	54851.169	$7.24 \cdot 10^{-9}$	$7.09 \cdot 10^{-9}$	$6.87 \cdot 10^{-9}$
	95032-04-05-00	54861.896	$1.38 \cdot 10^{-9}$	$1.18 \cdot 10^{-9}$	$1.35 \cdot 10^{-9}$
A 0535+26	94323-04-02-00	55176.507	$1.41 \cdot 10^{-7}$	$1.37 \cdot 10^{-7}$	$1.27 \cdot 10^{-7}$
	94323-05-03-01	55191.491	$4.73 \cdot 10^{-8}$	$4.30 \cdot 10^{-8}$	$4.08 \cdot 10^{-8}$
	94323-05-05-00	55207.573	$2.72 \cdot 10^{-10}$	$2.20 \cdot 10^{-10}$	$2.39 \cdot 10^{-10}$
GX 304-1	95417-01-03-02	55423.098	$3.52 \cdot 10^{-8}$	$2.99 \cdot 10^{-8}$	$3.30 \cdot 10^{-8}$
	95417-01-05-03	55432.113	$1.32 \cdot 10^{-8}$	$1.18 \cdot 10^{-8}$	$1.32 \cdot 10^{-8}$
	95417-01-06-03	55438.204	$1.09 \cdot 10^{-9}$	$1.01 \cdot 10^{-9}$	$1.10 \cdot 10^{-9}$
MXB 0656-072	80067-11-03-06	52949.541	$1.90 \cdot 10^{-8}$	$1.80 \cdot 10^{-8}$	$1.63 \cdot 10^{-8}$
	80430-01-04-02	52989.481	$3.44 \cdot 10^{-9}$	$3.3 \cdot 10^{-9}$	$3.14 \cdot 10^{-9}$
	80430-01-11-01	53038.742	$2.91 \cdot 10^{-10}$	$2.85 \cdot 10^{-10}$	$2.92 \cdot 10^{-10}$
EXO 2030+375	91089-01-12-05	53947.705	$4.1 \cdot 10^{-8}$	$3.7 \cdot 10^{-10}$	$3.3 \cdot 10^{-8}$
	91089-01-18-06	53991.793	$1.9 \cdot 10^{-8}$	$1.8 \cdot 10^{-8}$	$1.7 \cdot 10^{-8}$
	92067-01-09-03	54031.779	$9.3 \cdot 10^{-10}$	$8.27 \cdot 10^{-10}$	$9.3 \cdot 10^{-10}$
KS 1947+300	50425-01-24-00	51952.031	$8.76 \cdot 10^{-9}$	$8.07 \cdot 10^{-9}$	$7.55 \cdot 10^{-9}$
	60402-01-14-00	51996.078	$3.58 \cdot 10^{-9}$	$3.76 \cdot 10^{-9}$	$3.57 \cdot 10^{-9}$
	60402-01-31-00	52032.930	$7.76 \cdot 10^{-10}$	$6.92 \cdot 10^{-10}$	$7.48 \cdot 10^{-10}$
XTE 1543-564	50093-02-01-00	51629.945	$1.25 \cdot 10^{-9}$	$1.21 \cdot 10^{-9}$	$1.15 \cdot 10^{-9}$
	50093-02-13-01	51668.420	$5.20 \cdot 10^{-10}$	$4.98 \cdot 10^{-10}$	$5.15 \cdot 10^{-10}$
	50093-02-18-01	51685.856	$2.52 \cdot 10^{-10}$	$2.32 \cdot 10^{-10}$	$2.56 \cdot 10^{-10}$
XTE J1946+274	95032-12-01-00	55367.114	$5.00 \cdot 10^{-9}$	$4.63 \cdot 10^{-9}$	$4.15 \cdot 10^{-9}$
	95032-12-04-00	55387.031	$3.19 \cdot 10^{-9}$	$2.94 \cdot 10^{-9}$	$2.65 \cdot 10^{-9}$
	95032-12-08-00	55533.255	$1.64 \cdot 10^{-9}$	$1.50 \cdot 10^{-9}$	$1.43 \cdot 10^{-9}$
V 0332+53	90089-11-05-01	53364.911	$6.33 \cdot 10^{-8}$	$6.08 \cdot 10^{-8}$	$6.21 \cdot 10^{-8}$
	90014-01-04-02	53401.368	$2.12 \cdot 10^{-8}$	$2.05 \cdot 10^{-8}$	$2.14 \cdot 10^{-8}$
	90014-01-07-00	53424.367	$7.01 \cdot 10^{-10}$	$6.87 \cdot 10^{-10}$	$7.05 \cdot 10^{-10}$
4U 0115+634	93032-01-03-00	54556.253	$3.46 \cdot 10^{-8}$	$1.75 \cdot 10^{-8}$	$2.96 \cdot 10^{-8}$
	93032-01-05-01	54567.955	$3.11 \cdot 10^{-8}$	$9.26 \cdot 10^{-9}$	$2.97 \cdot 10^{-8}$
	93032-16-02-01	54578.359	$6.52 \cdot 10^{-9}$	$2.32 \cdot 10^{-9}$	$6.37 \cdot 10^{-9}$

Chapter 3: Data analysis

3.1 2S 1417-624

2S 1417-624 is a transient Be/X-ray binary that was detected first time in 1978 by Small Astronomy Sattelite 3 (SAS-3) (Apparao et al. 1980). Observations by Einstein satellite, identified a Be star as the optical companion, at the distance of 1.4-11.1 kpc (Grindlay et al. 1984). After a long period of quiescence, there was a giant outburst that lasted for 110 days, followed by five smaller Type I outbursts until the July of 1995. After the analysis of Burst and Transient Source Experiment observations of these outbursts, the orbital parameters were derived(Finger et al. 1996). After 4 years of quiescence, there was an other X-ray outburst in November of 1999, which was followed by four small outbursts between December of 1999 and August of 2000. The continuum spectrum was described with a power law with cutoff on higher energies. An iron line between 6.4 and 6.8 keV was detected, which led to the assumption that there was cold iron atoms with hydrogen or helium-like ionized gas around the pulsar (Inam et al. 2004). Since then, there were two giant outbursts in November 2009 and in November 2018.

Spectral fitting

We fitted the data from the outburst in November of 2009. We kept the iron line frozen on 6.4 keV, with a width of 0.1 keV. On the spectrum with the highest luminosity, the Bump and Reflection models improves the fit, giving statistically acceptable fits. The null hypothesis probabilities on this case are ~0. On the two spectra with lower luminosities, there is possibly no need for a gaussian or a reflection component to be added, since the null hypothesis probabilities are pretty high.

Table 3.1: The reduced chi-squared for each model and the F-test results: the probabilities for the null hypothesis to be true.

General Model	**Bump Model**		**Reflection model**	
χ^2 (d.o.f)	**F-test: probability**	**χ^2 (d.o.f)**	**F-test probability**	**χ^2 (d.o.f)**
2.02(41)	$2.6 \cdot 10^{-8}$	0.81(38)	$2.4 \cdot 10^{-10}$	0.75(40)
0.93(41)	0.71	0.97(38)	0.82	0.96(40)
0.93(42)	0.77	0.99(39)	0.31	0.96(41)

a) Obs-id: 94032-02-05-01

On the spectrum with the highest luminosity, the General model yielded a fit with a reduced chi-squared of 2.02(41) The fit can be improved by using the Bump model: adding a broad gaussian at 14.4 keV with a 4.8 keV width, gives a reduced chi-squared of 0.81 (38). Adding a reflection component with a scaling factor of -0.02 also improves the fit, by giving a reduced chi-squared of 0.75 (40).

Table 3.1a. Best fitting parameters of the three models and the fluxes. Energies are on keV, fluxes on erg cm^{-2} s^{-1} and normalizations on photons keV^{-1} cm^{-2} s^{-1}. Errors are quoted for 68% confidence level.

Parameters	**General model**	**Bump model**	**Reflection model**
χ^2(d.o.f)	2.02(41)	0.81(38)	0.75(40)
Γ	$0.25^{+0.01}_{-0.01}$	$0.37^{+0.04}_{-0.03}$	$0.18^{+0.01}_{-0.01}$
E_{cut}	$15.8^{+0.2}_{-0.3}$	16.9^{+1}_{-1}	$11.5^{+0.4}_{-0.3}$
$Normalization_{cutoffpl}$	$0.039^{+0.0004}_{-0.0005}$	$0.041^{+0.001}_{-0.002}$	$0.0330^{+0.0004}_{-0.0004}$
$Flux_{cutoffpl}$	$5.97 \cdot 10^{-9}$	$5.73 \cdot 10^{-9}$	$4.19 \cdot 10^{-9}$
E_{Fe}	6.4	6.4	6.4
EW_{Fe}	$0.064^{+0.006}_{-0.006}$	$0.06^{+0.01}_{-0.01}$	$0.04^{+0.01}_{-0.01}$
σ_{Fe}	0.1	0.1	0.1
$Normalization_{Fe}$	$0.0009^{+0.0001}_{-0.0001}$	$0.0009^{+0.0001}_{-0.0001}$	$0.0006^{+0.0001}_{-0.0001}$
E_{bump}	-	$14.4^{+0.9}_{-1.3}$	-
σ_{bump}	-	$4.8^{+2.6}_{-1.2}$	-
$Normalization_{bump}$	-	$0.006^{+0.009}_{-0.003}$	-
$Scaling\ Factor_{pexrav}$	-	-	$-0.020^{+0.005}_{-0.002}$
$Flux_{pexrav}$	-	-	$8.53 \cdot 10^{-10}$
Total Flux	$5.86 \cdot 10^{-9}$	$5.73 \cdot 10^{-9}$	$4.93 \cdot 10^{-9}$

b) Obs-id: 94444-01-03-01

The Bump and Reflection model does not improve the fit and thus there is no need for a gaussian or reflection component to be added to the model.

Table 3.1b. Best fitting parameters of the three models and the fluxes. Energies are on keV, fluxes on erg cm^{-2} s^{-1} and normalizations on photons keV^{-1} cm^{-2} s^{-1}. Errors are quoted for 68% confidence level.

Parameters	**General model**	**Bump model**	**Reflection model**
χ^2 (d.o.f)	0.93(41)	0.97(38)	0.96(40)
Γ	$0.17^{+0.02}_{-0.02}$	$0.19^{+0.04}_{-0.05}$	$0.16^{+0.01}_{-0.02}$
E_{cut}	$10.8^{+0.2}_{-0.2}$	$11.0^{+0.4}_{-0.2}$	$10.5^{+0.2}_{-0.4}$
$Norm_{cutoffpl}$	$0.0232^{+0.0004}_{-0.0004}$	$0.0238^{+0.0002}_{-0.0002}$	$0.0230^{+0.0001}_{-0.0002}$
$Flux_{cutoffpl}$	$2.69 \cdot 10^{-9}$	$2.69 \cdot 10^{-9}$	$2.63 \cdot 10^{-9}$
E_{fe}	6.4	6.4	6.4
EW_{Fe}	$0.05^{+0.01}_{-0.01}$	$0.06^{+0.01}_{-0.01}$	$0.05^{+0.01}_{-0.01}$
σ_{Fe}	0.1	0.1	0.1
$Normalization_{Fe}$	$0.0005^{+0.0001}_{-0.0001}$	$0.0005^{+0.0001}_{-0.0001}$	$0.00043^{+0.00007}_{-0.00007}$
E_{bump}	-	$12.4^{+0.5}_{-0.4}$	-
σ_{bump}	-	$1.0^{+1.0}_{-0.9}$	-
$Normalization_{bump}$	-	$0.0001^{+0.0001}_{-0.0001}$	-
Scaling $Factor_{pexrav}$	-	-	$-0.001^{+0.001}_{-0.002}$
$Flux_{pexrav}$	-	-	$3.89 \cdot 10^{-11}$
Total Flux	$2.60 \cdot 10^{-9}$	$2.60 \cdot 10^{-9}$	$2.57 \cdot 10^{-9}$

c) Obs-id: 94444-01-04-01

The Bump and Reflection model does not improve the fit and thus there is no need for a gaussian or reflection component to be added to the model.

Table 3.1c. Best fitting parameters of the three models and the fluxes. Energies are on keV, fluxes on erg cm^{-2} s^{-1} and normalizations on photons keV^{-1} cm^{-2} s^{-1}. Errors are quoted for 68% confidence level.

Parameters	General model	Bump model	Reflection model
χ^2 (d.o.f)	0.93(42)	0.99(39)	0.96(41)
Γ	$0.23^{+0.02}_{-0.02}$	$0.24^{+0.02}_{-0.02}$	$0.22^{+0.02}_{-0.02}$
E_{cut}	$10.5^{+0.2}_{-0.2}$	$10.5^{+0.3}_{-0.2}$	$10.2^{+0.2}_{-0.5}$
$Normalization_{cutoffpl}$	$0.0210^{+0.0004}_{-0.0004}$	$0.0211^{+0.0006}_{-0.0005}$	$0.0208^{+0.0004}_{-0.0004}$
$Flux_{cutoffpl}$	$1.93 \cdot 10^{-9}$	$1.93 \cdot 10^{-9}$	$1.89 \cdot 10^{-9}$
E_{Fe}	6.4	6.4	6.4
EW_{Fe}	$0.043^{+0.01}_{-0.01}$	$0.048^{+0.007}_{-0.009}$	$0.04^{+0.01}_{-0.01}$
σ_{Fe}	0.1	0.1	0.1
$Normalization_{Fe}$	$0.0003^{+0.0001}_{-0.0001}$	$0.0003^{+0.0001}_{-0.0001}$	$0.00030^{+0.00006}_{-0.00007}$
E_{bump}	-	$12.8^{+1.0}_{-2.2}$	-
σ_{bump}	-	$0.6^{+2.0}_{-0.6}$	-
$Normalization_{bump}$	-	$0.0001^{+0.0003}_{-0.0001}$	-
Scaling $Factor_{pexrav}$	-	-	$-0.001^{+0.001}_{-0.002}$
$Flux_{pexrav}$	-	-	$2.69 \cdot 10^{-9}$
Total Flux	$1.84 \cdot 10^{-9}$	$2.62 \cdot 10^{-9}$	$2.62 \cdot 10^{-9}$

3.2 4U 1901+03

4U 1901+03 is a transient Be/X-ray binary that was detected for the first time by the Uhuru and Vela 5B (Forman et al. 1976) in 1970-1971, when the system went into an outburst. The source was identified as an HMXB. It was not detected again until February of 2003 by the All-Sky Monitor (ASM) aboard RXTE (Galloway et al. 2003b). With a scan from the Proportional Counter Array (PCA), the precise coordinates of the source was able to be determined (Galloway et al. 2003). The 2003 outburst lasted for about five months. During that period, the luminosity changed almost three orders of magnitude, from ~ $10^{38}\,\mathrm{erg\,sec^{-1}}$ to ~ $10^{35}\,\mathrm{erg\,sec^{-1}}$. The spectrum was described by an absorbed power law with exponential cut-off (Molkov et al. 2003; James et al. 2011) or a model consistent with thermal Comptonization (Galloway et al. 2005), but there were residuals. From data obtained from RXTE, the 10 keV feature was found (Reig et al. 2016), which was fitted as an absorption feature. An iron line was also present at ~6.4 keV. An optical or IR counterpart has yet to be found (Galloway et al. 2005). The distance was assumed to be ~10 kpc (Galloway et al. 2005). In 2009, the first phase-resolved spectra analysis was presented, with data from the 2003 outburst, from RXTE (Lei et al. 2009). It was found that the iron line at 6.4 keV did not vary with pulse profile, which indicates that it's origin lies in the accretion disk. In 2011, there was a short and weak outburst. It was detected by MAXI/GSC (Sootome et al. 2011) and Fermi/GBM (Jenke & Finger 2011).

Spectral fitting

We fitted the data from the outburst of 2003. We kept the iron line frozen on 6.4 keV, with a width of 0.5 keV. The Bump model improves the fit significantly for all luminosities. The Reflection model's fits were problematic but also improves the fit. The probabilities of the null hypothesis are ~0 except for the Reflection model's fit on the spectrum with the highest luminosity which was ~0.1.

Table 3.2: The reduced chi-squared for each model and the F-test results: the probabilities for the null hypothesis to be true

General Model	**Bump Model**		**Reflection model**	
χ^2 (d.o.f)	**F-test: probability**	**χ^2 (d.o.f)**	**F-test probability**	**χ^2 (d.o.f)**
3.53(42)	$8.7\cdot10^{-9}$	1.47(40)	0.14	3.43(41)
6.12(42)	$1.8\cdot10^{-15}$	1.04(39)	$1.3\cdot10^{-10}$	2.27(41)
3.64(42)	$1.0\cdot10^{-13}$	0.98(41)	$1.9\cdot10^{-6}$	2.18(41)

a) Obs-id: 70096-01-03-04

On the most luminous spectrum, the General model did a poor fit, giving a reduced chi-squared of 3.53(42). By adding a broad gaussian at 15 keV with a width of 5.7 keV, the fit becomes statistically acceptable. The energy of the gaussian was kept frozen, since it took unacceptable values when kept free. The Bump model on this case gives a reduced chi-squared of 1.47(40). The Reflection model with a scaling factor of -0.13 does a slightly better fit, giving a reduced chi-squared of 3.43(41).

Table 3.2a. Best fitting parameters of the three models and the fluxes. Energies are on keV, fluxes on erg cm^{-2} s^{-1} and normalizations on photons keV^{-1} cm^{-2} s^{-1}. Errors are quoted for 68% confidence level.

Parameters	General model	Bump model	Reflection model
χ^2 (d.o.f)	3.53(42)	1.47(40)	3.43(41)
Γ	$0.67^{+0.02}_{-0.02}$	$-0.13^{+0.04}_{-0.04}$	$0.64^{+0.01}_{-0.01}$
E_{cut}	$7.9^{+0.1}_{-0.1}$	$3.9^{+0.2}_{-0.2}$	$7.3^{+0.2}_{-0.2}$
$Normalization_{cutoffpl}$	$0.507^{+0.007}_{-0.007}$	$0.25^{+0.01}_{-0.01}$	$0.495^{+0.007}_{-0.007}$
$Flux_{cutoffpl}$	$1.03 \cdot 10^{-8}$	$7.46 \cdot 10^{-9}$	$9.66 \cdot 10^{-9}$
E_{fe}	6.4	6.4	6.4
EW_{Fe}	$0.17^{+0.01}_{-0.01}$	$0.14^{+0.01}_{-0.01}$	$0.16^{+0.01}_{-0.01}$
σ_{Fe}	0.5	0.5	0.5
$Normalization_{Fe}$	$0.0101^{+0.0005}_{-0.0005}$	$0.0088^{+0.0006}_{-0.0006}$	$0.0100^{+0.0006}_{-0.0006}$
E_{bump}	-	15	-
σ_{bump}	-	$5.7^{+0.1}_{-0.1}$	-
$Normalization_{bump}$	-	$0.063^{+0.004}_{-0.004}$	-
Scaling $Factor_{pexrav}$	-	-	$-0.13^{+0.05}_{-0.05}$
$Flux_{pexrav}$	-	-	$4.56 \cdot 10^{-10}$
Total Flux	$8.75 \cdot 10^{-9}$	$8.12 \cdot 10^{-9}$	$8.63 \cdot 10^{-9}$

b) Obs-id: 70096-01-16-01

On the second spectrum, the General model gives a poor fit of a reduced chi-squared of 6.12(42). Both Reflection and Bump model improves the fit: by adding a broad gaussian at 15 keV with a 3.6 keV width, the reduced chi-squared becomes equal to 1.04(39). By adding a reflection component with a scaling factor of -0.74, the reduced chi-squared goes to 2.27(41), which is an improvement but it still makes for a poor fit. The flux of the iron line tends to go to zero values.

Table 3.2b. Best fitting parameters of the three models and the fluxes. Energies are on keV, fluxes on erg cm^{-2} s^{-1} and normalizations on photons keV^{-1} cm^{-2} s^{-1}. Errors are quoted for 68% confidence level.

Parameters	**General model**	**Bump model**	**Reflection model**
χ^2(d.o.f)	6.12(42)	1.04(39)	2.27(41)
Γ	$1.41^{+0.01}_{-0.01}$	$1.31^{+0.05}_{-0.03}$	$1.25^{+0.01}_{-0.01}$
E_{cut}	$19.9^{+0.7}_{-0.6}$	$13.1^{+1.2}_{-1.5}$	$9.9^{+0.3}_{-0.2}$
$Normalization_{cutoffpl}$	$0.445^{+0.007}_{-0.007}$	$0.43^{+0.01}_{-0.01}$	$0.389^{+0.006}_{-0.006}$
$Flux_{cutoffpl}$	$4.76 \cdot 10^{-9}$	$4.11 \cdot 10^{-9}$	$9.33 \cdot 10^{-10}$
E_{fe}	6.4	6.4	Not detected
EW_{Fe}	$0.04^{+0.01}_{-0.01}$	$0.05^{+0.01}_{-0.01}$	-
σ_{Fe}	0.5	0.5	-
$Normalization_{Fe}$	$0.0010^{+0.0002}_{-0.0002}$	$0.0012^{+0.0002}_{-0.0002}$	-
E_{bump}	-	15	-
σ_{bump}	-	$3.6^{+0.5}_{-0.5}$	-
$Normalization_{bump}$	-	$0.0077^{+0.0007}_{-0.0006}$	-
Scaling $Factor_{pexrav}$	-	-	$-0.74^{+0.06}_{-0.06}$
$Flux_{pexrav}$	-	-	$8.51 \cdot 10^{-10}$
Total Flux	$3.91 \cdot 10^{-9}$	$3.47 \cdot 10^{9}$	$3.43 \cdot 10^{-9}$

c) Obs-id: 70096-01-21-00

On the spectrum with the lowest luminosity, the General model gives a fit with a reduced chi-squared of 3.64(42), which can again be improved with both the Bump and the Reflection model, by giving a chi-squared of 0.98(41) and 2.18(41) respectively. In this case, the broad gaussian is at 12.7 keV, with a width of 5 keV which was kept frozen since it couldn't be constrained and the scaling factor on the Reflection model is -0.32. The iron line ,this time , is not detected with both the General and the Reflection models. The only fit that can be considered statistically acceptable is the one done by the phenomenological model.

Table 3.2c. Best fitting parameters of the three models and the fluxes. Energies are on keV, fluxes on erg cm^{-2} s^{-1} and normalizations on photons keV^{-1} cm^{-2} s^{-1}. Errors are quoted for 68% confidence level.

Parameters	**General model**	**Bump model**	**Reflection model**
χ^2 (d.o.f)	3.64(42)	0.98(41)	2.18(41)
Γ	$1.718^{+0.005}_{-0.005}$	$1.97^{+0.02}_{-0.02}$	$1.49^{+0.02}_{-0.02}$
E_{cut}	500	500	$16.45^{+1.0}_{-0.9}$
$Normalization_{cutoffpl}$	$0.176^{+0.002}_{-0.002}$	$0.270^{+0.007}_{-0.007}$	$0.138^{+0.004}_{-0.003}$
$Flux_{cutoffpl}$	$2.20 \cdot 10^{-9}$	$2.20 \cdot 10^{-9}$	$1.08 \cdot 10^{-9}$
E_{fe}	Not detected	6.4	Not detected
EW_{Fe}	-	$0.06^{+0.02}_{-0.02}$	-
σ_{Fe}	-	0.5	-
$Normalization_{Fe}$	-	$0.0004^{+0.0001}_{-0.0001}$	-
E_{bump}	-	$12.7^{+0.2}_{-0.2}$	-
σ_{bump}	-	5	-
$Normalization_{bump}$	-	$0.0067^{+0.0006}_{-0.0006}$	-
Scaling $Factor_{pexrav}$	-	-	$-0.32^{+0.04}_{-0.05}$
$Flux_{pexrav}$	-	-	$4.45 \cdot 10^{-10}$
Total Flux	$1.99 \cdot 10^{-9}$	$1.62 \cdot 10^{-9}$	$1.41 \cdot 10^{-9}$

3.3 1A 1118-61

1A 1118-61 is a transient Be/X-ray binary system, that was detected first time by the satellite Ariel-5 (Eyles et al. 1975), during an outburst that lasted for ~10 days, in 1974. The optical counterpart was identified as the Be-star He 3-640/Wray 793 (Chevalier & Ilovaisky 1975). The distance was estimated to be ~5 kpc (Janor-Pacheco et al. 1981), which was later confirmed (Coe & Payne 1985 et al.). The X-ray spectrum was fitted with a power law. In 1992, a second outburst with about the same flux as the first outburst, was observed by Burst and Transient Source Experiment (BATSE) on the Compton Gamma Ray Observatory (CGRO) in 1991-1992. After this incident, the system was in quiescence for almost 20 years, until there was an outburst in January of 2009, that lasted for ~20 days and it was first observed by Swift/XRT. After about three weeks, the International Gamma-ray Astrophysics Laboratory (INTEGRAL/JEM-X/ISGRI) observed flaring activity. Many observations were carried out with RXTE/PCA and HEXTE (see section 2.1). A cyclotron absorption feature was found at ~55 keV, which indicates a magnetic field strength of $4.8 \cdot 10^{12}$ G (Doroshenko et al. 2010). An iron fluorescent line was observed at ~6.4 keV(e.g. Devasia 2010 et al.). A peculiar absorption feature was detected at ~8 keV, with a width of ~0.1 keV (Rothschild et al. 2008, Doroshenko et al. 2010). Suchy et al. (2011) detected the 10 keV feature, which was described by a negative broad gaussian component.

Spectral fitting

We used the data from the outburst in January of 2009. The iron line was kept frozen at 6.4 keV, while it's width was left free when fitting the spectrum with the highest luminosity. It was kept frozen on the other two, at 0.5 keV, based on the results from fitting the first one. The Bump and Reflection models improve the fits, based on the results of the F-test for the highest luminosity, which are ~0 and 0.01 respectively. On the lower luminosities, it's questionable where there is an improvement or not, with the null hypothesis probabilities being 0.17 and 0.07 respectively for the second spectrum, and 0.19 for the Bump model, on the third. The Reflection model on the lowest luminosity does not improve the fit at all.

Table 3.3: The reduced chi-squared for each model and the F-test results: the probabilities for the null hypothesis to be true.

General Model	**Bump Model**		**Reflection model**	
χ^2 (d.o.f)	**F-test: probability**	**χ^2 (d.o.f)**	**F-test probability**	**χ^2 (d.o.f)**
1.55(41)	$4.2 \cdot 10^{-6}$	0.81(38)	0.01	1.29(39)
1.10(42)	0.17	1.02(39)	0.07	1.04(41)
1.65(43)	0.19	1.47(38)	1	1.73(42)

a) Obs-id: 94032-04-02-09

On the first spectrum, the fits made by all three models are statistically acceptable. The General model makes a fit with a chi-squared of 1.55(41), which can be improved by adding a broad gaussian on 18.6 keV, with a width of 5.3 keV or by adding a reflection component with a scaling factor of -0.016. The chi-squared on each case is 0.81(38) and 1.29(39) respectively.

Table 3.3a. Best fitting parameters of the three models and the fluxes. Energies are on keV, fluxes on erg cm^{-2} s^{-1} and normalizations on photons keV^{-1} cm^{-2} s^{-1}. Errors are quoted for 68% confidence level.

Parameters	General model	Bump model	Reflection model
χ^2 (d.o.f)	1.55(41)	0.81(38)	1.29(39)
Γ	$0.13^{+0.01}_{-0.01}$	$-0.05^{+0.02}_{-0.03}$	$0.10^{+0.02}_{-0.02}$
E_{cut}	$12.0^{+0.1}_{-0.1}$	$8.9^{+0.4}_{-0.4}$	$10.8^{+0.3}_{-0.3}$
$Normalization_{cutoffpl}$	$0.0803^{+0.0008}_{-0.0008}$	$0.070^{+0.002}_{-0.001}$	$0.079^{+0.003}_{-0.003}$
$Flux_{cutoffpl}$	$1.25 \cdot 10^{-8}$	$1.15 \cdot 10^{-8}$	$1.11 \cdot 10^{-8}$
E_{fe}	6.4	6.4	6.4
EW_{Fe}	$0.15^{+0.01}_{-0.02}$	$0.12^{+0.01}_{-0.01}$	$0.14^{+0.03}_{-0.01}$
σ_{Fe}	$0.53^{+0.07}_{-0.07}$	$0.41^{+0.07}_{-0.07}$	$0.59^{+0.09}_{-0.09}$
$Normalization_{Fe}$	$0.0054^{+0.0006}_{-0.0006}$	$0.0046^{+0.0004}_{-0.0004}$	$0.0050^{+0.0004}_{-0.0004}$
E_{bump}	-	$18.6^{+0.2}_{-0.2}$	-
σ_{bump}	-	$5.3^{+1.6}_{-1.0}$	-
$Normalization_{bump}$	-	$0.025^{+0.001}_{-0.008}$	-
Scaling $Factor_{pexrav}$	-	-	$-0.016^{+0.005}_{-0.005}$
$Flux_{pexrav}$	-	-	$7.66 \cdot 10^{-10}$
Total Flux	$1.21 \cdot 10^{-8}$	$1.13 \cdot 10^{-8}$	$1.15 \cdot 10^{-8}$

b) Obs-id: 94032-04-03-05

On the second spectrum, the General model makes a good fit of a reduced chi-squared of 1.10(42). Both the Bump and Reflection models slightly improves the fit. By adding a broad gaussian at 16.4 keV with a width of 2.9 keV, the reduced chi-squared goes to 1.02(39). By adding a reflection component with a scaling factor of -0.014, the reduced chi-squared goes to 1.04(41).

Table 3.3b. Best fitting parameters of the three models and the fluxes. Energies are on keV, fluxes on erg cm^{-2} s^{-1} and normalizations on photons keV^{-1} cm^{-2} s^{-1}. Errors are quoted for 68% confidence level.

Parameters	General model	Bump model	Reflection model
χ^2 (d.o.f)	1.10(42)	1.02(39)	1.04(41)
Γ	$0.38^{+0.01}_{-0.01}$	$0.38^{+0.01}_{+0.01}$	$0.34^{+0.02}_{-0.02}$
E_{cut}	$13.97^{+0.2}_{-0.2}$	$13.59^{+0.3}_{-0.3}$	$12.4^{+0.7}_{-0.6}$
$Normalization_{cutoffpl}$	$0.075^{+0.001}_{-0.001}$	$0.076^{0.001}_{-0.001}$	$0.073^{+0.001}_{-0.001}$
$Flux_{cutoffpl}$	$7.50 \cdot 10^{-9}$	$7.31 \cdot 10^{-9}$	$6.71 \cdot 10^{-9}$
E_{Fe}	6.4	6.4	6.4
EW_{Fe}	$0.127^{+0.004}_{-0.008}$	$0.124^{+0.010}_{-0.008}$	$0.117^{+0.020}_{-0.007}$
σ_{Fe}	0.5	0.5	0.5
$Normalization_{Fe}$	$0.0030^{+0.0002}_{-0.0002}$	$0.0029^{+0.0002}_{-0.0002}$	$0.0028^{+0.0003}_{-0.0003}$
E_{bump}	-	$16.4^{+0.9}_{-0.7}$	-
σ_{bump}	-	$2.9^{+0.9}_{-0.5}$	-
$Normalization_{bump}$	-	$0.0013^{+0.0003}_{-0.0003}$	-
$Scaling\ Factor_{pexrav}$	-	-	$-0.014^{+0.007}_{-0.007}$
$Flux_{pexrav}$	-	-	$4.01 \cdot 10^{-10}$
Total Flux	$7.24 \cdot 10^{-9}$	$7.09 \cdot 10^{-9}$	$6.87 \cdot 10^{-9}$

c) Obs-id: 95032-04-05-00

On the spectrum with the lowest luminosity, the Bump model slightly improves the fit. The reduced chi-squared with the General model is 1.65(43) which goes to 1.47(38) by fitting the data with the Bump model. The broad gaussian is at 18.6 keV with a width of 3.7 keV. The Reflection model does not improve the fit at all.

Table 3.3c. Best fitting parameters of the three models and the fluxes. Energies are on keV, fluxes on erg cm^{-2} s^{-1} and normalizations on photons keV^{-1} cm^{-2} s^{-1}. Errors are quoted for 68% confidence level.

Parameters	**General model**	**Bump model**	**Reflection model**
χ^2 (d.o.f)	1.65(43)	1.47(38)	1.73(42)
Γ	$0.98^{+0.03}_{-0.03}$	$0.7^{+0.1}_{-0.1}$	$0.91^{+0.03}_{-0.04}$
E_{cut}	$16.39^{+1.1}_{-1.0}$	$9.90^{+1.5}_{-2.0}$	$14.93^{+0.9}_{-1.7}$
$Normalization_{cutoffpl}$	$0.064^{+0.002}_{-0.002}$	$0.050^{+0.005}_{-0.003}$	$0.056^{+0.002}_{-0.002}$
$Flux_{cutoffpl}$	$1.58 \cdot 10^{-9}$	$1.30 \cdot 10^{-9}$	$1.52 \cdot 10^{-9}$
E_{Fe}	6.4	6.4	6.4
EW_{Fe}	$0.10^{+0.02}_{-0.02}$	$0.07^{+0.02}_{-0.03}$	$0.12^{+0.02}_{-0.03}$
σ_{Fe}	0.5	0.5	0.5
$Normalization_{Fe}$	$0.0007^{+0.0001}_{-0.0001}$	$0.0005^{+0.0002}_{-0.0002}$	$0.0008^{+0.0001}_{-0.0001}$
E_{bump}		$18.6^{+0.8}_{-0.6}$	
σ_{bump}		$3.7^{+1.5}_{-0.9}$	
$Normalization_{bump}$		$0.002^{+0.003}_{-0.001}$	
$Scaling\ Factor_{pexrav}$			$-0.001^{+0.001}_{-0.009}$
$Flux_{pexrav}$			$6.61 \cdot 10^{-12}$
Total Flux	$1.38 \cdot 10^{-9}$	$1.18 \cdot 10^{-9}$	$1.35 \cdot 10^{-9}$

3.4 A 0535+26

A 0535+26 is a transient Be/X-ray binary which was discovered by the satellite Ariel 5 during an outburst in April of 1975 (Rosenberg et al. 1975). It's optical companion HDE 245770 is a Be star (Li et al. 1979) with a distance of ~2 kpc (Steele et al. 1998, Gaia Collaboration 2016). The orbital parameters are also derived (Finger et al. 1996). After the discovery of the system through the first outburst, the system has went through a couple of giant outbursts until 1994, where it went in to quiescence for ~ 10 years. In 2005, it went though an outburst, which peaked in May/June of 2005 and was followed by two small ones (type I). In 2008/2009 a couple of small outbursts occurred, with a big outburst in between, in May of 2009. An fluorescent iron line was detected at 6.4 keV (Caballero et al. 2013). Since then, there were two big outbursts, in February of 2011 and one in January of 2015. The spectrum has been fitted with a cut-off power law with an additional blackbody component (e.g. Caballero et al. 2013). It has two cyclotron resonant scattering features (CRSF), the one at ~ 50 keV, and the second harmonic at ~ 100 keV (Kendziorra et al. 1994; Grove et al. 1995; Kretschmar et al. 1996).

Spectral fitting

We used the data from the outburst in 2009. The iron line was kept frozen at 6.4 keV. It's width was left free while fitting the data on the highest luminosity spectrum. It was kept frozen at 0.3 keV while fitting the data on the spectra with the lower luminosities, a value based on the results of fitting the data with the highest luminosity. On all cases, the Bump and Reflection models do significantly better fits. The F-test results gives ~0 probabilities for the null hypothesis to be true. The reduced chi-squared for the Bump and Reflection model are between the values of ~0.4-0.8 (except for the fit with the Reflection model on the data with the lowest luminosity), which indicates that we may have overestimated the errors.

Table 3.4: The reduced chi-squared for each model and the F-test results: the probabilities for the null hypothesis to be true.

General Model	**Bump Model**		**Reflection model**	
χ^2 (d.o.f)	**F-test: probability**	**χ^2 (d.o.f)**	**F-test probability**	**χ^2 (d.o.f)**
2.76(41)	$5.5 \cdot 10^{-12}$	0.70(38)	$5.8 \cdot 10^{-15}$	0.61(40)
6.46(42)	$5.6 \cdot 10^{-22}$	0.52(39)	$1.3 \cdot 10^{-20}$	0.78(41)
1.32(42)	$6.6 \cdot 10^{-10}$	0.45(39)	0.03	1.21(41)

a) Obs-id: 94323-04-02-00

On the spectrum with the highest luminosity, the General model does a poor fit of a reduced chi-squared of 2.76(41). Both the Bump and Reflection model fit the data. The Bump model gives a reduced chi-squared of 0.70(38). The broad gaussian for the Bump model is at 15 keV with a width of 5.2 keV. The Reflection model with a scaling factor of -0.34, gives a reduced chi-squared of 0.61(40).

Table 3.4a. Best fitting parameters of the three models and the fluxes. Energies are on keV, fluxes on erg cm^{-2} s^{-1} and normalizations on photons keV^{-1} cm^{-2} s^{-1}. Errors are quoted for 68% confidence level.

Parameters	General model	Bump model	Reflection model
χ^2 (d.o.f)	2.76(41)	0.70(38)	0.61(40)
Γ	$0.179^{+0.006}_{-0.006}$	$0.27^{+0.02}_{-0.02}$	$0.153^{+0.007}_{-0.007}$
E_{cut}	$14.2^{+0.1}_{-0.1}$	$14.8^{+0.5}_{-1.0}$	$11.6^{+0.2}_{-0.2}$
$Normalization_{cutoffpl}$	$0.776^{+0.006}_{-0.006}$	$0.91^{+0.02}_{-0.02}$	$0.778^{+0.006}_{-0.006}$
$Flux_{cutoffpl}$	$1.41 \cdot 10^{-7}$	$1.35 \cdot 10^{-7}$	$1.09 \cdot 10^{-7}$
E_{fe}	6.4	6.4	6.4
EW_{Fe}	$0.122^{+0.007}_{-0.005}$	$0.12^{+0.01}_{-0.01}$	$0.10^{+0.01}_{-0.01}$
σ_{Fe}	$0.30^{+0.06}_{-0.06}$	$0.35^{+0.07}_{-0.07}$	$0.29^{+0.07}_{-0.08}$
$Normalization_{Fe}$	$0.044^{+0.002}_{-0.002}$	$0.046^{+0.003}_{-0.003}$	$0.036^{+0.003}_{-0.002}$
E_{bump}	-	$15.0^{+0.7}_{-1.2}$	-
σ_{bump}	-	$5.2^{+2.6}_{-1.3}$	-
$Normalization_{bump}$	-	$0.13^{+0.20}_{-0.07}$	-
Scaling $Factor_{pexrav}$	-	-	$-0.34^{+0.04}_{-0.04}$
$Flux_{pexrav}$	-	-	$1.71 \cdot 10^{-8}$
Total Flux	$1.41 \cdot 10^{-7}$	$1.37 \cdot 10^{-7}$	$1.27 \cdot 10^{-7}$

b) Obs-id: 94323-05-03-01

On the second spectrum, the General model does a poor fit of a reduced chi-squared of 6.46(42). The Bump model fits the data with a reduced chi-squared of 0.52(39). The broad gaussian is at 15.9 keV with a width of 5.9 keV. The Reflection model with a scaling factor of -0.36, fits the data with a reduced chi-squared of 0.78(41).

Table 3.4b. Best fitting parameters of the three models and the fluxes. Energies are on keV, fluxes on erg cm^{-2} s^{-1} and normalizations on photons keV^{-1} cm^{-2} s^{-1}. Errors are quoted for 68% confidence level.

Parameters	General model	Bump model	Reflection model
χ^2 (d.o.f)	6.46(42)	0.52(39)	0.78(41)
Γ	$0.388^{+0.006}_{-0.006}$	$0.44^{+0.02}_{-0.05}$	$0.363^{+0.006}_{-0.006}$
E_{cut}	$15.4^{+0.2}_{-0.1}$	$13.5^{+1.6}_{-2.0}$	$11.3^{+0.2}_{-0.2}$
$Normalization_{cutoffpl}$	$0.433^{+0.003}_{-0.003}$	$0.503^{+0.008}_{-0.009}$	$0.450^{+0.004}_{-0.004}$
$Flux_{cutoffpl}$	$4.75 \cdot 10^{-8}$	$4.20 \cdot 10^{-8}$	$3.33 \cdot 10^{-8}$
E_{fe}	6.4	6.4	6.4
EW_{Fe}	$0.060^{+0.005}_{-0.005}$	$0.058^{+0.006}_{-0.004}$	$0.024^{+0.005}_{-0.004}$
σ_{Fe}	0.3	0.3	0.3
$Normalization_{Fe}$	$0.0076^{+0.0007}_{-0.0007}$	$0.0081^{+0.0008}_{-0.0006}$	$0.0034^{+0.0007}_{-0.0006}$
E_{bump}	-	$15.9^{+0.3}_{-1.6}$	-
σ_{bump}	-	$5.9^{+3.1}_{-1.5}$	-
$Normalization_{bump}$	-	$0.115^{+0.003}_{-0.004}$	-
Scaling $Factor_{pexrav}$	-	-	$-0.36^{+0.03}_{-0.03}$
$Flux_{pexrav}$	-	-	$7.85 \cdot 10^{-9}$
Total Flux	$4.73 \cdot 10^{-8}$	$4.30 \cdot 10^{-8}$	$4.08 \cdot 10^{-8}$

c) Obs-id: 94323-05-05-00

On the spectrum with the lowest luminosity, the General model fits the data, with a reduced chi-squared of 1.32(42). Both the Bump and Reflection models improve the fit. Adding a broad gaussian at 18.6 keV with a width of 3.9 keV, the reduced chi-squared goes to 0.45(39). By adding a reflection component with a scaling factor of -0.04, the reduced chi-squared goes to 1.21(41).

Table 3.4c. Best fitting parameters of the three models and the fluxes. Energies are on keV, fluxes on erg cm^{-2} s^{-1} and normalizations on photons keV^{-1} cm^{-2} s^{-1}. Errors are quoted for 68% confidence level.

Parameters	General model	Bump model	Reflection model
χ^2 (d.o.f)	1.32(42)	0.45(39)	1.21(41)
Γ	$1.57^{+0.08}_{-0.08}$	$1.4^{+0.1}_{-0.1}$	$1.48^{+0.09}_{-0.09}$
E_{cut}	$30.8^{+15.0}_{-7.8}$	$10.4^{+1.9}_{-1.4}$	$13.8^{+5.4}_{-2.9}$
$Normalization_{cutoffpl}$	$0.028^{+0.002}_{-0.002}$	$0.030^{+0.003}_{-0.003}$	$0.027^{+0.002}_{-0.002}$
$Flux_{cutoffpl}$	$2.65 \cdot 10^{-10}$	$2.33 \cdot 10^{-10}$	$2.03 \cdot 10^{-10}$
E_{fe}	6.4	6.4	6.4
EW_{Fe}	$0.186^{+0.026}_{-0.030}$	$0.08^{+0.03}_{-0.03}$	$0.115^{+0.027}_{-0.25}$
σ_{Fe}	0.3	0.3	0.3
$Normalization_{Fe}$	$0.00020^{+0.00004}_{-0.00004}$	$0.00010^{+0.00005}_{-0.00005}$	$0.00015^{+0.00004}_{-0.00004}$
E_{bump}	-	$18.6^{+1.5}_{-0.9}$	-
σ_{bump}	-	$3.9^{+1.2}_{-0.7}$	-
$Normalization_{bump}$	-	$0.0010^{+0.0003}_{-0.0002}$	-
Scaling $Factor_{pexrav}$	-	-	$-0.04^{+0.02}_{-0.03}$
$Flux_{pexrav}$	-	-	$4.29 \cdot 10^{-11}$
Total Flux	$2.69 \cdot 10^{-10}$	$2.21 \cdot 10^{-10}$	$2.37 \cdot 10^{-10}$

3.5. GX 304-1

The transient Be/X-ray binary GX 304-1 was first discovered during hard X-ray balloon observations in 1967 (e.g. McClintock et al. 1971). It's spectrum was described by an absorbed power law (White et al. 1983). A Be star was identified as the optical counterpart (Mason et al. 1978) and it's distance was measured to be ~2.4 kpc (Parkes et al. 1980). Since 1980, the system went in to quiescence until June of 2008. The INTEGRAL sattelite detected hard X-rays from the source (Manousakis et al. 2008) and since then, several outbursts has been detected with the Swift Burst Alert Telescope (BAT) and the Monitor of All-Sky Image (MAXI) (Yamamoto et al. 2009, 2012; Krimm et al. 2010; Mihara et al. 2010). Using RXTE Proportional Counter Array (PCA) observations during it's outburst in 2010, Devasia described the spectrum with a partial covering high-energy cut-off power law (Devasia et al. 2011). An fluorescent iron line was detected (e.g. Devasia et al. 2011). A cyclotron absorption feature was detected at ~54 keV (Yamamoto et al. 2011) as we The orbital parameters has been determined (Sugizaki et al. 2015) with data from a series of outbursts from 2009 to 2013 observed by MAXI/GSC, RXTE/PCA, and Fermi/Gamma-Ray Burst Monitor (GBM).

Spectral fitting

We used the data from an outburst in August of 2010. The iron line was kept frozen at 6.4 keV with a width of 0.5 keV. The Bump model do significantly better fits on all spectra. The null hypothesis probabilities calculated with the F-test are almost zero. On the spectrum with the highest luminosity, the Reflection model also fit the data, with an almost zero null hypothesis probability, but on the other two, there is no need for a reflection component to be included to the model, since the null hypothesis probabilities are equal to 1 on both cases.

Table 3.5: The reduced chi-squared for each model and the F-test results: the probabilities for the null hypothesis to be true.

General Model	**Bump Model**		**Reflection model**	
χ^2 (d.o.f)	**F-test: probability**	**χ^2 (d.o.f)**	**F-test probability**	**χ^2 (d.o.f)**
2.41(42)	$1.3 \cdot 10^{-9}$	0.84(39)	$6.0 \cdot 10^{-6}$	1.49(41)
1.89(43)	$1.8 \cdot 10^{-7}$	0.87(40)	1	1.96(42)
1.73(42)	$8.5 \cdot 10^{-5}$	1.21(41)	1	1.78(41)

a) Obs-id: 95417-01-03-02

On the spectrum with the highest luminosity, the General model does a poor fit with a reduced chi-squared of 2.41(42). By adding a broad gaussian at 17.5 keV with a width of 6.3 keV, the reduced chi-squared goes to 0.84(39). By adding a reflection component with a scaling factor equal to -0.26, the reduced chi-squared goes to 1.49(41).

Table 3.5a. Best fitting parameters of the three models and the fluxes. Energies are on keV, fluxes on erg cm^{-2} s^{-1} and normalizations on photons keV^{-1} cm^{-2} s^{-1}. Errors are quoted for 68% confidence level.

Parameters	**General model**	**Bump model**	**Reflection model**
χ^2 (d.o.f)	2.41(42)	0.84(39)	1.49(41)
Γ	$0.68^{+0.02}_{-0.02}$	$0.45^{+0.07}_{-0.05}$	$0.639^{+0.008}_{-0.008}$
E_{cut}	$14.8^{+0.2}_{-0.2}$	$9.5^{+1.5}_{-0.4}$	$12.5^{+0.3}_{-0.3}$
$Normalization_{cutoffpl}$	$0.76^{+0.02}_{-0.02}$	$0.64^{+0.01}_{-0.02}$	$0.757^{+0.006}_{-0.006}$
$Flux_{cutoffpl}$	$3.72 \cdot 10^{-8}$	$2.84 \cdot 10^{-8}$	$3.21 \cdot 10^{-8}$
E_{fe}	6.4	6.4	6.4
EW_{Fe}	$0.121^{+0.006}_{-0.008}$	$0.115^{+0.009}_{-0.009}$	$0.103^{+0.007}_{-0.007}$
σ_{Fe}	0.5	0.5	0.5
$Normalization_{Fe}$	$0.017^{+0.001}_{-0.001}$	$0.016^{+0.001}_{-0.001}$	$0.015^{+0.001}_{-0.001}$
E_{bump}	-	$17.5^{+0.4}_{-0.7}$	-
σ_{bump}	-	$6.3^{+0.4}_{-2.5}$	-
$Normalization_{bump}$	-	$0.115^{+0.004}_{-0.004}$	-
$Rel\text{-}ref_{pexrav}$	-	-	$-0.26^{+0.04}_{-0.04}$
$Flux_{pexrav}$	-	-	$3.02 \cdot 10^{-9}$
Total Flux	$3.52 \cdot 10^{-8}$	$2.99 \cdot 10^{-8}$	$3.30 \cdot 10^{-8}$

b) Obs-id: 95417-01-05-03

On the second spectrum, the General model fits the data, with a chi-squared of 1.89(43). The Bump model improves the fit. In this case, the broad gaussian is at 17 keV, with a width of 7.5 keV. There is no need for a reflection component to be added to the model.

Table 3.5b. Best fitting parameters of the three models and the fluxes. Energies are on keV, fluxes on erg cm^{-2} s^{-1} and normalizations on photons keV^{-1} cm^{-2} s^{-1}. Errors are quoted for 68% confidence level.

Parameters	**General model**	**Bump model**	**Reflection model**
χ^2 (d.o.f)	1.89(43)	0.87(40)	1.96(42)
Γ	$0.865^{+0.009}_{-0.009}$	$0.37^{+0.07}_{-0.09}$	$0.875^{+0.009}_{-0.009}$
E_{cut}	$12.7^{+0.2}_{-0.2}$	$6.4^{+0.8}_{-1.0}$	$12.87^{+0.2}_{-0.2}$
$Normalization_{cutoffpl}$	$0.590^{+0.006}_{-0.006}$	$0.37^{+0.01}_{-0.01}$	$0.600^{+0.006}_{-0.006}$
$Flux_{cutoffpl}$	$1.32 \cdot 10^{-8}$	$1.05 \cdot 10^{-8}$	$1.46 \cdot 10^{-8}$
E_{fe}	6.4	6.4	6.4
EW_{Fe}	$0.08^{+0.01}_{-0.01}$	$0.06^{+0.01}_{-0.01}$	$0.08^{+0.01}_{-0.01}$
σ_{Fe}	0.5	0.5	0.5
$Normalization_{Fe}$	$0.0060^{+0.0005}_{-0.0005}$	$0.0045^{+0.0006}_{-0.0006}$	$0.0060^{+0.0005}_{-0.0005}$
E_{bump}	-	$17.0^{+1.3}_{-3.9}$	-
σ_{bump}	-	$7.5^{+2.5}_{-1.5}$	-
$Normalization_{bump}$	-	$0.08^{+0.09}_{-0.03}$	-
$Rel\text{-}ref_{pexrav}$	-	-	$-0.001^{+0.001}_{-0.008}$
$Flux_{pexrav}$	-	-	~0
Total Flux	$1.32 \cdot 10^{-8}$	$1.18 \cdot 10^{-8}$	$1.32 \cdot 10^{-8}$

c) Obs-id: 95417-01-06-03

On the spectrum with the lowest luminosity, the General model fits the data, with a reduced chi-squared of 1.73(42). The Bump model improves the fit, with a chi-squared of 1.21(41). The broad gaussian is at 17.5 keV, with a width of 7.5 keV. Both parameters were kept frozen since they couldn't be constrained on logical values. There is no need for a reflection component to be concluded to the model.

Table 3.5c. Best fitting parameters of the three models and the fluxes. Energies are on keV, fluxes on erg cm^{-2} s^{-1} and normalizations on photons keV^{-1} cm^{-2} s^{-1}. Errors are quoted for 68% confidence level.

Parameters	General model	Bump model	Reflection model
χ^2 (d.o.f)	1.73(42)	1.21(41)	1.78(41)
Γ	$1.66^{+0.06}_{-0.06}$	$0.73^{+0.2}_{-0.2}$	$1.69^{+0.06}_{-0.06}$
E_{cut}	$20.0^{+2.7}_{-2.1}$	$5.3^{+0.7}_{-0.6}$	$21.2^{+2.7}_{-2.1}$
$Normalization_{cutoffpl}$	$0.22^{+0.02}_{-0.02}$	$0.09^{+0.02}_{-0.02}$	$0.23^{+0.01}_{-0.03}$
$Flux_{cutoffpl}$	$1.09 \cdot 10^{-9}$	$9.02 \cdot 10^{-10}$	$1.42 \cdot 10^{-9}$
E_{fe}	6.4	6.4	6.4
EW_{Fe}	$0.10^{+0.02}_{-0.02}$	$0.06^{+0.02}_{-0.02}$	$0.10^{+0.03}_{-0.02}$
σ_{Fe}	0.5	0.5	0.5
$Normalization_{Fe}$	$0.0007^{+0.0001}_{-0.0001}$	$0.0004^{+0.0001}_{-0.0002}$	$0.0007^{+0.0001}_{-0.0001}$
E_{bump}	-	17.5	-
σ_{bump}	-	7.5	-
$Normalization_{bump}$	-	$0.0080^{+0.0009}_{-0.0009}$	-
$Rel\text{-}ref_{pexrav}$	-	-	$-0.001^{+0.001}_{-0.010}$
$Flux_{pexrav}$	-	-	~0
Total Flux	$1.09 \cdot 10^{-9}$	$1.01 \cdot 10^{-9}$	$1.10 \cdot 10^{-9}$

3.6 MXB 0656-072

The transient Be/X-ray binary MXB 0656-072 was detected in September of 1975 by SAS-3 (Clark et al. 1975) and in the next year, was observed twice with Ariel V. The system remained unobserved, until the October of 2003, when it went through a big outburst which lasted for over 2 months. The optical counterpart was identified as a O9.7Ve star (Pakull et al. 2003). A CRSF was found at ~35 keV, that implies a magnetic field strength of $3.7 \cdot 10^{12}$ G and the spectrum was fit with a power law with an exponential cut-off (Heindl et al. 2003). An iron fluorescent line was detected (e.g. Nespoli et al. 2012). Also, the 10 keV feature has been detected for this source, with data obtained from RXTE (McBride et al. 2006, Nespoli et al. 2012) and was fitted as an absoprion feature, along with an Iron line at 6.4 keV. Between 2007 and 2008, a series of outbursts was reported by INTEGRAL (Kreykenbohmet et al. 2007), RXTE/ASM (Pottschmidt et al .2007) and Swift/BAT (Kennea et al. 2007). The orbital parameters have been determined (Jingzhi Yan et al. 2012).

Spectral fitting

We took the data from the outburst in 2003. The iron line was kept frozen at 6.4 keV, with a width of 0.5 keV. We included the cyclotron line and we kept it frozen at 35 keV with a width of 6 keV. The Bump model improves the fit on the first two spectra but not on the one with the lowest luminosity. The null hypothesis for these two cases are almost zero and 0.02 respectively. The Reflection model improves the fit only for the spectrum with the highest luminosity, having a ~0 null hypothesis probability.

Table 3.6: The reduced chi-squared for each model and the F-test results: the probabilities for the null hypothesis to be true.

General Model	**Bump Model**		**Reflection model**	
χ^2 (d.o.f)	**F-test: probability**	**χ^2 (d.o.f)**	**F-test probability**	**χ^2 (d.o.f)**
6.07(41)	$3.0 \cdot 10^{-7}$	2.76(38)	0.008	4.67(40)
2.05(42)	0.02	1.66(39)	0.80	2.02(41)
0.89(43)	0.76	0.91(40)	1	0.92(42)

a) Obs-id: 80067-11-03-06

On the spectrum with the highest luminosity, the General model does an unacceptable fit of a reduced chi-squared of 6.07(41). By adding a broad gaussian at 15.2 keV with a 2.2 keV width, the reduced chi-squared goes to 2.76(38). By adding a reflection component, with a scaling factor of -0.34, the reduced chi-reduced goes to 4.67(40).

Table 3.6a. Best fitting parameters of the three models and the fluxes. Energies are on keV, fluxes on erg cm^{-2} s^{-1} and normalizations on photons keV^{-1} cm^{-2} s^{-1}. Errors are quoted for 68% confidence level.

Parameters	General model	Bump model	Reflection model
χ^2 (d.o.f)	6.07(41)	2.76(38)	4.67(40)
Γ	$0.68^{+0.01}_{-0.01}$	$0.66^{+0.04}_{-0.05}$	$0.57^{+0.02}_{-0.02}$
E_{cut}	$21.1^{+0.7}_{-0.7}$	$16.65^{+0.9}_{-2.1}$	$11.7^{+0.7}_{-0.8}$
$Normalization_{cutoffpl}$	$0.356^{+0.005}_{-0.005}$	$0.38^{+0.01}_{-0.01}$	$0.355^{+0.005}_{-0.005}$
$Flux_{cutoffpl}$	$1.90 \cdot 10^{-8}$	$2.28 \cdot 10^{-8}$	$1.63 \cdot 10^{-8}$
E_{fe}	6.4	6.4	6.4
EW_{Fe}	$0.46^{+0.01}_{-0.01}$	$0.42^{+0.02}_{-0.02}$	$0.36^{+0.02}_{-0.01}$
σ_{Fe}	0.5	0.5	0.5
$Normalization_{Fe}$	$0.0348^{+0.0007}_{-0.0007}$	$0.032^{+0.001}_{-0.001}$	$0.029^{+0.001}_{-0.001}$
E_{bump}	-	$15.2^{+0.2}_{-0.2}$	-
σ_{bump}	-	$2.2^{+0.4}_{-0.4}$	-
$Normalization_{bump}$	-	$0.012^{+0.007}_{-0.004}$	-
$Rel\text{-}ref_{pexrav}$	-	-	$-0.34^{+0.06}_{-0.05}$
$Flux_{pexrav}$	-	-	$4.23 \cdot 10^{-9}$
E_{gabs}	35	35	35
σ_{gabs}	6	6	6
Strength	$68.7^{+2.9}_{-2.9}$	$36.5^{+9.0}_{-11.4}$	$44.6^{+4.7}_{-4.6}$
Total Flux	$1.90 \cdot 10^{-8}$	$1.80 \cdot 10^{-8}$	$1.63 \cdot 10^{-8}$

b) Obs-id: 80430-01-04-02

On the second spectrum, the General model does a poor fit or 2.05(42). The Bump model on this case improves the fit. The reduced chi-squared goes to 1.66(39). The broad gaussian is at ~15.2 keV with a width of 2.2 keV. The Reflection model does not improve the fit.

Table 3.6b. Best fitting parameters of the three models and the fluxes. Energies are on keV, fluxes on erg cm^{-2} s^{-1} and normalizations on photons keV^{-1} cm^{-2} s^{-1}. Errors are quoted for 68% confidence level.

Parameters	**General model**	**Bump model**	**Reflection model**
χ^2 (d.o.f)	2.05(42)	1.66(39)	2.02(41)
Γ	$1.20^{+0.02}_{-0.02}$	$1.03^{+0.07}_{-0.06}$	$1.03^{+0.04}_{-0.03}$
E_{cut}	$27.0^{+2.4}_{-2.1}$	$15.6^{+2.7}_{-2.4}$	$14.3^{+2.5}_{-1.8}$
$Normalization_{cutoffpl}$	$0.221^{+0.005}_{-0.005}$	$0.192^{+0.009}_{-0.009}$	$0.188^{+0.005}_{-0.005}$
$Flux_{cutoffpl}$	$7.93 \cdot 10^{-9}$	$4.03 \cdot 10^{-9}$	$3.61 \cdot 10^{-9}$
E_{fe}	6.4	6.4	6.4
EW_{Fe}	$0.35^{+0.01}_{-0.01}$	$0.32^{+0.02}_{-0.02}$	$0.31^{+0.02}_{-0.03}$
σ_{Fe}	0.5	0.5	0.5
$Normalization_{Fe}$	$0.0065^{+0.0003}_{-0.0002}$	$0.0065^{+0.0003}_{-0.0003}$	$0.0058^{+0.0004}_{-0.0004}$
E_{bump}	-	$15.2^{+0.3}_{-0.3}$	-
σ_{bump}	-	$2.2^{+0.5}_{-0.5}$	-
$Normalization_{bump}$	-	$0.002^{+0.002}_{-0.001}$	-
$Rel\text{-}ref_{pexrav}$	-	-	$-0.11^{+0.04}_{-0.05}$
$Flux_{pexrav}$	-	-	$5.00 \cdot 10^{-10}$
E_{gabs}	35	35	35
σ_{gabs}	6	6	6
Strength	$66.9^{+6.8}_{-6.6}$	$22.9^{+14.3}_{-15.3}$	$46.6^{+9.0}_{-5.0}$
Total Flux	$3.44 \cdot 10^{-9}$	$3.3 \cdot 10^{-9}$	$3.14 \cdot 10^{-9}$

c) Obs-id: 80430-01-11-01

The Bump and Reflection model does not improve the fit and thus there is no need for a gaussian or reflection component to be added to the model. Width of the broad gaussian on the Bump model was frozen on the best fit value, since it couldn't be constrained on logical values.

Table 3.6c. Best fitting parameters of the three models and the fluxes. Energies are on keV, fluxes on erg cm^{-2} s^{-1} and normalizations on photons keV^{-1} cm^{-2} s^{-1}. Errors are quoted for 68% confidence level.

Parameters	**General model**	**Bump model**	**Reflection model**
χ^2 (d.o.f)	0.89(43)	0.91(40)	0.92(42)
Γ	$1.31^{+0.07}_{-0.07}$	$0.9^{+0.2}_{-0.3}$	$1.37^{+0.07}_{-0.07}$
E_{cut}	$10.3^{+1.0}_{-1.2}$	$6.6^{+2.1}_{-2.1}$	$10.9^{+1.3}_{-1.3}$
$Normalization_{cutoffpl}$	$0.053^{+0.004}_{-0.003}$	$0.038^{+0.006}_{-0.006}$	$0.058^{+0.004}_{-0.004}$
$Flux_{cutoffpl}$	$4.06 \cdot 10^{-10}$	$3.56 \cdot 10^{-10}$	$4.16 \cdot 10^{-10}$
E_{fe}	6.4	6.4	6.4
EW_{Fe}	$0.15^{+0.03}_{-0.03}$	$0.13^{+0.05}_{-0.03}$	$0.15^{+0.05}_{-0.05}$
σ_{Fe}	0.5	0.5	0.5
$Normalization_{Fe}$	$0.00040^{+0.00008}_{-0.00008}$	$0.0003^{+0.0001}_{-0.0001}$	$0.00040^{+0.00009}_{-0.00007}$
E_{bump}	-	$16.5^{+1.4}_{-1.5}$	-
σ_{bump}	-	5	-
$Normalization_{bump}$	-	$0.0007^{+0.0006}_{-0.0005}$	-
$Rel\text{-}ref_{pexrav}$	-	-	$-0.001^{+0.001}_{-0.010}$
$Flux_{pexrav}$	-	-	$3.03 \cdot 10^{-13}$
E_{gabs}	35	35	35
σ_{gabs}	6	6	6
Strength	20	20	20
Total Flux	$2.91 \cdot 10^{-10}$	$2.85 \cdot 10^{-10}$	$2.92 \cdot 10^{-10}$

3.7 EXO 2030+375

The transient Be/X-ray binary EXO 2030+375 was discovered in 1985 with the European X-ray Observatory Satellite (EXOSAT), during a big outburst (Parmar, White & Stella 1989b). The optical counterpart was discovered at a distance of 7.1 kpc (Motch & Janot-Pacheco 1987; Coe 1988; Wilson et al. 2002) and identified as a Be star. The orbital parameters were also derived (Stollberg 1997) by using long term BATSE monitoring data. The system goes through a type I outburst on every periastron passage (Wilson et al. 2002). In June of 2006, there was a big outburst which laster for about 140 days (Krimm et al. 2006). After this event, the small outbursts continued but since 2015, the system is less active. The spectrum has been described with an absorbed power law with a high energy cut-off (Reig & Coe 1999; Wilson, Finger & Camero-Arranz 2008). An iron fluorescent line has been detected on 6.4 ke (e.g. Epili et al. 2018). The 10 keV feature was detected and fitted by adding a partial covering component to the model. The detection of cyclotron absorption fatures has been reported at ~11, 36 and 63 keV, with data obtained from RXTE and INTEGRAL (Reig & Coe 1999; Wilson, Finger & Camero-Arranz 2008), but on the data from Suzaku, taken on type I outbursts in the periods of May-June of 2007 and May of 2012, no such features were detected.

Spectral fitting

We took the data from the outburst in 2006. We kept the iron line frozen at 6.4 keV with a width of 0.5 keV. Both Bump and Reflection models improve the fit on the first two spectra, with null hypothesis probabilities of ~0. On the spectrum with the lowest luminosity, the Bump model improves the fit, since the null hypothesis probability is 0.001, but the Reflection model does not. It is possible that we overestimated the errors, since the reduced chi-squared on the last spectrum take values of ~0.5-0.7.

Table 3.7: The reduced chi-squared for each model and the F-test results: the probabilities for the null hypothesis to be true.

General Model	**Bump Model**		**Reflection model**	
χ^2 (d.o.f)	**F-test: probability**	**χ^2 (d.o.f)**	**F-test probability**	**χ^2 (d.o.f)**
8.10(42)	$1.67 \cdot 10^{-14}$	1.58(39)	$9.67 \cdot 10^{-11}$	2.95(41)
3.15(42)	$1.08 \cdot 10^{-9}$	1.09(39)	$1.28 \cdot 10^{-10}$	1.16(41)
0.69(42)	0.001	0.50(39)	1	0.71(41)

a) Obs-id: 91089-01-12-05

On the spectrum with the highest luminosity, the General model does a poor fit of a reduced chi-squared of 8.10(42). The Bump model, with a broad gaussian at 15.6 keV with a 2.9 keV width, improves the fit, with a reduced chi-squared of 1.58(39). The Reflection model does a poor but improved fit, with a chi-reduced of 2.95(41). The scaling factor on this case is -5.8.

Table 3.7a. Best fitting parameters of the three models and the fluxes. Energies are on keV, fluxes on erg cm^{-2} s^{-1} and normalizations on photons keV^{-1} cm^{-2} s^{-1}. Errors are quoted for 68% confidence level.

Parameters	**General model**	**Bump model**	**Reflection model**
χ^2 (d.o.f)	8.10(42)	1.58(39)	2.95(41)
Γ	$1.700^{+0.008}_{-0.008}$	$1.72^{+0.02}_{-0.01}$	$1.607^{+0.008}_{-0.008}$
E_{cut}	$87.79^{+7.6}_{-6.5}$	$59.82^{+8.3}_{-8.8}$	$20.6^{+0.8}_{-0.7}$
$Normalization_{cutoffpl}$	$4.30^{+0.04}_{-0.04}$	$4.63^{+0.06}_{-0.06}$	$4.17^{+0.05}_{-0.05}$
$Flux_{cutoffpl}$	$4.5 \cdot 10^{-8}$	$4.2 \cdot 10^{-8}$	$3.00 \cdot 10^{-8}$
E_{fe}	6.4	6.4	6.4
EW_{Fe}	$0.146^{+0.007}_{-0.008}$	$0.145^{+0.008}_{-0.007}$	$0.087^{+0.01}_{-0.01}$
σ_{Fe}	0.5	0.5	0.5
$Normalization_{Fe}$	$0.025^{+0.001}_{-0.001}$	$0.025^{+0.001}_{-0.001}$	$0.015^{+0.001}_{-0.001}$
E_{bump}	-	$15.6^{+0.2}_{-0.2}$	-
σ_{bump}	-	$2.9^{+0.4}_{-0.3}$	-
$Normalization_{bump}$	-	$0.025^{+0.006}_{-0.004}$	-
$Rel\text{-}ref_{pexrav}$	-	-	$-5.8^{+0.5}_{-0.5}$
$Flux_{pexrav}$	-	-	$7.6 \cdot 10^{-9}$
Total Flux	$4.05 \cdot 10^{-8}$	$3.73 \cdot 10^{-8}$	$3.26 \cdot 10^{-8}$

b) Obs-id: 91089-01-18-06

On the second spectrum, the General model does a poor fit of 3.15(42), which can be improved by both the Bump and Reflection model. By adding a broad gaussian at 13.8 keV with a width of 4.5 keV, the reduced chi-squared goes to 1.09(39). By adding a reflection component with a scaling factor of -0.84, the reduced chi-squared goes to 1.16(41).

Table 3.7b. Best fitting parameters of the three models and the fluxes. Energies are on keV, fluxes on erg cm^{-2} s^{-1} and normalizations on photons keV^{-1} cm^{-2} s^{-1}. Errors are quoted for 68% confidence level.

Parameters	General model	Bump model	Reflection model
χ^2(d.o.f)	3.15(42)	1.09(39)	1.16(41)
Γ	$1.07^{+0.01}_{-0.01}$	$1.13^{+0.02}_{-0.04}$	$0.98^{+0.01}_{-0.01}$
E_{cut}	$16.9^{+0.3}_{-0.3}$	$16.5^{+1.1}_{-2.2}$	$11.2^{+0.3}_{-0.3}$
$Normalization_{cutoffpl}$	$0.96^{+0.01}_{-0.01}$	$1.08^{+0.01}_{-0.01}$	$0.91^{+0.01}_{-0.01}$
$Flux_{cutoffpl}$	$1.99 \cdot 10^{-8}$	$1.89 \cdot 10^{-8}$	$1.51 \cdot 10^{-8}$
E_{fe}	6.4	6.4	6.4
EW_{Fe}	$0.108^{+0.009}_{-0.009}$	$0.12^{+0.01}_{-0.01}$	$0.07^{+0.01}_{-0.01}$
σ_{Fe}	0.5	0.5	0.5
$Normalization_{Fe}$	$0.0098^{+0.0007}_{-0.0007}$	$0.0109^{+0.0007}_{-0.0007}$	$0.0061^{+0.0008}_{-0.0008}$
E_{bump}	-	$13.8^{+0.7}_{-0.6}$	-
σ_{bump}	-	$4.5^{+0.5}_{-0.4}$	-
$Normalization_{bump}$	-	$0.023^{+0.002}_{-0.002}$	-
$Rel\text{-}ref_{pexrav}$	-	-	$-0.84^{+0.09}_{-0.01}$
$Flux_{pexrav}$	-	-	$2.86 \cdot 10^{-9}$
Total Flux	$1.89 \cdot 10^{-8}$	$1.82 \cdot 10^{-8}$	$1.72 \cdot 10^{-8}$

c) Obs-id: 92067-01-09-03

On the spectrum with the lowest luminosity, all three models fit the data, but with values for the reduced chi-squared of ~0.5 – 0.7. That indicates an overestimation of the errors. As for the model parameters, the broad gaussian is at 18.3 keV with a 4.3 keV width, and the scaling factor is -0.001.

Table 3.7c. Best fitting parameters of the three models and the fluxes. Energies are on keV, fluxes on erg cm^{-2} s^{-1} and normalizations on photons keV^{-1} cm^{-2} s^{-1}. Errors are quoted for 68% confidence level.

Parameters	General model	Bump model	Reflection model
χ^2 (d.o.f)	0.69(42)	0.50(39)	0.71(41)
Γ	$1.05^{+0.06}_{-0.06}$	$0.4^{+0.2}_{-0.3}$	$1.04^{+0.06}_{-0.06}$
E_{cut}	$12.9^{+1.3}_{-1.1}$	$5.9^{+1.2}_{-1.6}$	$12.6^{+1.3}_{-1.3}$
$Normalization_{cutoffpl}$	$0.067^{+0.004}_{-0.004}$	$0.034^{+0.004}_{-0.005}$	$0.066^{+0.004}_{-0.003}$
$Flux_{cutoffpl}$	$1.10 \cdot 10^{-9}$	$8.24 \cdot 10^{-10}$	$1.09 \cdot 10^{-9}$
E_{fe}	6.4	6.4	6.4
EW_{Fe}	$0.086^{+0.02}_{-0.02}$	$0.05^{+0.04}_{-0.04}$	$0.09^{+0.6}_{-0.4}$
σ_{Fe}	0.5	0.5	0.5
$Normalization_{Fe}$	$0.0005^{+0.0002}_{-0.0002}$	$0.0003^{+0.0002}_{-0.0002}$	$0.0005^{+0.0002}_{-0.0002}$
E_{bump}	-	$18.3^{+1.1}_{-2.5}$	-
σ_{bump}	-	$4.3^{+3.9}_{-1.3}$	-
$Normalization_{bump}$	-	$0.003^{+0.007}_{-0.001}$	-
$Rel\text{-}ref_{pexrav}$	-	-	$-0.001^{+0.001}_{-0.010}$
$Flux_{pexrav}$	-	-	$1.65 \cdot 10^{-12}$
Total Flux	$9.34 \cdot 10^{-10}$	$8.27 \cdot 10^{-10}$	$9.30 \cdot 10^{-10}$

3.8 KS 1947+300

The transient Be/X-ray binaty KS 1947+300 was first observed in June of 1989 from the Mir space station, with the Kvant/TTM coded-mask X-ray spectrometer (Skinner 1989, Borozdin et al. 1990). An absorbed power law was used to fit the data (Borozdin et al. 1990). A Be star was discovered as the optical counterpart, at a distance of ~10 kpc (Negueruela et al. 2003). The source was in quiescence from 1995 to 2000, until it went through an outburst. Using data from RXTE, the spectrum was described with a Comptonization continuum model with a blackbody component (Galloway et al. 2004). . An iron fluorescent line was detected at 6.5 keV (Galloway et al. 2004). The orbital parameters were determined (Galloway et al. 2004). From BeppoSax observations of the outburst in 2001, an emission line from helium-like iron atoms was detected at 6.7 keV, but the Kα line was absent. The source went through a number of small outbursts, from 2002 to 2004, with the strongest one in April of 2004, where the spectrum was described by a power law with a high-energy cutoff, using the data obtained from the observations of the INTEGRAL/ISGRI and JEM-X (Tsygankov & Lutovinov 2005). The next big outburst occurred in October of 2013. With combined spectra from NuSTAR and Swift/XRT, the spectrum was described by a power law with a high energy exponential cut-off. An iron fluorescent line was detected at 6.5 keV, and a cyclotron line at ~12.2 keV. The cyclotron line has not been detected with any other observatory.

Spectral fitting

We used the data from the outburst in 2001. The iron line was kept frozen at 6.4 keV with a width of 0.1 keV. The Bump model improves the fit on the first two spectra, since the F-test gives null hypothesis probabilities of ~0 and 0.002 respectively. The Reflection model improves the fit only on the spectrum with the highest luminosity, where the F-test gives a null hypothesis probability of ~0. On all the other cases, the null hypothesis probability is equal to 1.

Table 3.8: The reduced chi-squared for each model and the F-test results: the probabilities for the null hypothesis to be true.

General Model	**Bump Model**		**Reflection model**	
χ^2 (d.o.f)	**F-test: probability**	**χ^2 (d.o.f)**	**F-test probability**	**χ^2 (d.o.f)**
1.64(42)	$8.64 \cdot 10^{-7}$	0.85(40)	$4.10 \cdot 10^{-5}$	1.11(41)
1.66(42)	0.002	1.29(40)	1	1.71(41)
1.56(42)	1	1.59(40)	1	1.59(41)

a) Obs-id: 50425-01-24-00

On the spectrum with the highest luminosity, all models fit the data. The General model yields a fit with a reduced chi-squared of 1.64(42). The Bump model improves the fit with a broad gaussian at 14.7 keV with a 5 keV width, and the Reflection model with a scaling factor of -0.21. The reduced chi-squared for each model respectively is 0.85(40) and 1.11(41). The width of the broad gaussian on the Bump model was kept frozen, since it couldn't be constrained on logical values.

Table 3.8a. Best fitting parameters of the three models and the fluxes. Energies are on keV, fluxes on erg cm^{-2} s^{-1} and normalizations on photons keV^{-1} cm^{-2} s^{-1}. Errors are quoted for 68% confidence level.

Parameters	General model	Bump model	Reflection model
χ^2 (d.o.f)	1.64(42)	0.85(40)	1.11(41)
Γ	$1.16^{+0.01}_{-0.01}$	$1.15^{+0.03}_{-0.03}$	$1.09^{+0.01}_{-0.01}$
E_{cut}	$31.2^{+1.3}_{-1.2}$	$25.7^{+3.0}_{-2.6}$	$17.9^{+1.4}_{-1.1}$
$Normalization_{cutoffpl}$	$0.315^{+0.004}_{-0.004}$	$0.320^{+0.008}_{-0.008}$	$0.307^{+0.004}_{-0.004}$
$Flux_{cutoffpl}$	$8.75 \cdot 10^{-9}$	$7.85 \cdot 10^{-9}$	$6.38 \cdot 10^{-9}$
E_{Fe}	6.4	6.4	6.4
EW_{Fe}	$0.054^{+0.006}_{-0.006}$	$0.06^{+0.01}_{-0.01}$	$0.02^{+0.01}_{-0.01}$
σ_{Fe}	0.1	0.1	0.1
$Normalization_{Fe}$	$0.0016^{+0.0002}_{-0.0002}$	$0.0019^{+0.0002}_{-0.0002}$	$0.0008^{+0.0003}_{-0.0003}$
E_{bump}	-	$14.7^{+0.8}_{-1.0}$	-
σ_{bump}	-	5	-
$Normalization_{bump}$	-	$0.008^{+0.02}_{-0.02}$	-
$Rel\text{-}ref_{pexrav}$	-	-	$-0.21^{+0.04}_{-0.04}$
$Flux_{pexrav}$	-	-	$1.15 \cdot 10^{-9}$
Total Flux	$8.76 \cdot 10^{-9}$	$8.07 \cdot 10^{-9}$	$7.55 \cdot 10^{-9}$

b) Obs-id: 60402-01-14-00

On the second spectra, the General model fit the data with a reduced chi-squared of 1.66(42). The Bump model improves the fit with a broad gaussian at 8.7 keV and a 5 keV width, that was again kept frozen. The reduced chi-squared goes to 1.29(40). The Reflection model does not improve the fit.

Table 3.8b. Best fitting parameters of the three models and the fluxes. Energies are on keV, fluxes on erg cm^{-2} s^{-1} and normalizations on photons keV^{-1} cm^{-2} s^{-1}. Errors are quoted for 68% confidence level.

Parameters	**General model**	**Bump model**	**Reflection model**
χ^2 (d.o.f)	1.66(42)	1.29(40)	1.71(41)
Γ	$0.74^{+0.02}_{-0.02}$	$0.93^{+0.08}_{-0.07}$	$0.74^{+0.02}_{-0.02}$
E_{cut}	$14.85^{+0.5}_{-0.5}$	$20.14^{+4.0}_{-2.8}$	$14.8^{+0.5}_{-0.9}$
$Normalization_{cutoffpl}$	$0.086^{+0.002}_{-0.002}$	$0.103^{+0.006}_{-0.006}$	$0.086^{+0.002}_{-0.002}$
$Flux_{cutoffpl}$	$3.57 \cdot 10^{-9}$	$3.61 \cdot 10^{-9}$	$3.56 \cdot 10^{-9}$
E_{Fe}	6.4	6.4	6.4
EW_{Fe}	$0.01^{+0.01}_{-0.01}$	$0.039^{+0.01}_{-0.01}$	$0.01^{+0.01}_{-0.01}$
σ_{Fe}	0.1	0.1	0.1
$Normalization_{Fe}$	$0.0002^{+0.0002}_{-0.0002}$	$0.0006^{+0.0002}_{-0.0002}$	$0.0002^{+0.0002}_{-0.0002}$
E_{bump}	-	$8.7^{+0.7}_{-0.6}$	-
σ_{bump}	-	5	-
$Normalization_{bump}$	-	$0.010^{+0.003}_{-0.004}$	-
$Rel\text{-}ref_{pexrav}$	-	-	$-0.001^{+0.001}_{-0.008}$
$Flux_{pexrav}$	-	-	$1.01 \cdot 10^{-11}$
Total Flux	$3.58 \cdot 10^{-9}$	$3.76 \cdot 10^{-9}$	$3.57 \cdot 10^{-9}$

c) Obs-id: 60402-01-31-00

The Bump and Reflection model does not improve the fit and thus there is no need for a gaussian or reflection component to be added to the model.

Table 3.8c. Best fitting parameters of the three models and the fluxes. Energies are on keV, fluxes on erg cm^{-2} s^{-1} and normalizations on photons keV^{-1} cm^{-2} s^{-1}. Errors are quoted for 68% confidence level.

Parameters	**General model**	**Bump model**	**Reflection model**
χ^2 (d.o.f)	1.56(42)	1.59(40)	1.59(41)
Γ	$0.39^{+0.04}_{-0.04}$	$0.05^{+0.10}_{-0.10}$	$0.32^{+0.05}_{-0.05}$
E_{cut}	$10.14^{+0.5}_{-0.5}$	$6.79^{+1.2}_{-0.9}$	$9.0^{+0.5}_{-1.0}$
$Normalization_{cutoffpl}$	$0.0135^{+0.0006}_{-0.0006}$	$0.098^{+0.001}_{-0.001}$	$0.0128^{+0.0006}_{-0.0006}$
$Flux_{cutoffpl}$	$7.89 \cdot 10^{-10}$	$6.23 \cdot 10^{-10}$	$7.10 \cdot 10^{-10}$
E_{Fe}	6.4	6.4	6.4
EW_{Fe}	$0.11^{+0.01}_{-0.01}$	$0.11^{+0.03}_{-0.01}$	$0.10^{+0.02}_{-0.02}$
σ_{Fe}	0.1	0.1	0.1
$Normalization_{Fe}$	$0.00040^{+0.00007}_{-0.00007}$	$0.00038^{+0.00007}_{-0.00007}$	$0.0004^{+0.0002}_{-0.0002}$
E_{bump}	-	$17.5^{+1.5}_{-0.9}$	-
σ_{bump}	-	5	-
$Normalization_{bump}$	-	$0.002^{+0.001}_{-0.001}$	-
$Rel\text{-}ref_{pexrav}$	-	-	$-0.003^{+0.003}_{-0.004}$
$Flux_{pexrav}$	-	-	$4.63 \cdot 10^{-11}$
Total Flux	$7.76 \cdot 10^{-10}$	$6.92 \cdot 10^{-10}$	$7.48 \cdot 10^{-10}$

3.9 XTE J1543-568

XTE J1548-568 is a transient Be/X-ray binary that was first discovered with the PCA instrument of RXTE, on February of 2000 (Marshall, Takeshima & In ’t Zand 2000). After the discovery, the pulsar was found on earlier data as well by BATSE, from Januay of 2000 (Finger & Wilson 2000). It’s location was determined (Kaptein, In ’t Zand & Heise 2001). The orbital parameters were determined and it’s distance to be more than 10 kpc (J.J.M. in ’t Zand et al. 2001). For years, it’s optical companion remained undetected, until H.A Krimm et al. (2012) tentatively identified a star inside the XRT error circle, as it. On the same publication, the brightening of the source was reported. It’s spectrum was described by an absorbed power law.

Spectral fitting

We took the data from the outburst in 2000. The iron line was kept frozen at 6.4 keV with a width of 0.4 keV. On all spectra, all three models fit the data. However, the F-test gave quite high null hypothesis probabilities, and in one case on the second spectra, the null hypothesis for the Reflection model is 1. In all of them, the reduced chi-square's value is lower than 1, so the errors could have been overestimated.

Table 3.9: The reduced chi-squared for each model and the F-test results: the probabilities for the null hypothesis to be true.

General Model	**Bump Model**		**Reflection model**	
χ^2 (d.o.f)	**F-test: probability**	**χ^2 (d.o.f)**	**F-test probability**	**χ^2 (d.o.f)**
0.91(42)	0.24	0.89(39)	0.22	0.90(41)
0.86(42)	0.48	0.87(41)	1	0.89(41)
0.49(42)	0.04	0.43(40)	0.08	0.46(41)

a) Obs-id: 50093-02-01-00

On the spectrum with the highest luminosity, the General model fit the data with a reduced chi-squared of 0.91(42). The Bump model gives a reduced chi-squared of 0.89(39). The broad gaussian for the Bump model is at 17 keV with a width of 1.1 keV. The Reflection model with a scaling factor of -0.006, gives a reduced chi-squared of 0.90(41).

Table 3.9a. Best fitting parameters of the three models and the fluxes. Energies are on keV, fluxes on erg cm^{-2} s^{-1} and normalizations on photons keV^{-1} cm^{-2} s^{-1}. Errors are quoted for 68% confidence level.

Parameters	**General model**	**Bump model**	**Reflection model**
χ^2 (d.o.f)	0.91(42)	0.89(39)	0.90(41)
Γ	$0.29^{+0.05}_{-0.05}$	$0.02^{+0.05}_{-0.06}$	$0.20^{+0.06}_{-0.06}$
E_{cut}	$11.6^{+0.7}_{-0.7}$	$10.7^{+0.8}_{-0.8}$	$9.3^{+1.6}_{-1.0}$
$Normalization_{cutoffpl}$	$0.0138^{+0.0007}_{-0.0007}$	$0.0133^{+0.0008}_{-0.0004}$	$0.0128^{+0.0007}_{-0.0006}$
$Flux_{cutoffpl}$	$1.29 \cdot 10^{-9}$	$1.22 \cdot 10^{-9}$	$1.04 \cdot 10^{-9}$
E_{Fe}	6.4	6.4	6.4
EW_{Fe}	$0.14^{+0.02}_{-0.02}$	$0.13^{+0.04}_{-0.03}$	$0.12^{+0.04}_{-0.03}$
σ_{Fe}	0.4	0.4	0.4
$Normalization_{Fe}$	$0.0006^{+0.0001}_{-0.0001}$	$0.0006^{+0.00007}_{-0.00007}$	$0.0004^{+0.0002}_{-0.0002}$
E_{bump}	-	$17.0^{+0.8}_{-0.8}$	-
σ_{bump}	-	$1.1^{+1.0}_{-0.9}$	-
$Normalization_{bump}$	-	$0.0003^{+0.0003}_{-0.0002}$	-
$Rel\text{-}ref_{pexrav}$	-	-	$-0.006^{+0.005}_{-0.005}$
$Flux_{pexrav}$	-	-	$1.39 \cdot 10^{-10}$
Total Flux	$1.25 \cdot 10^{-9}$	$1.21 \cdot 10^{-9}$	$1.15 \cdot 10^{-9}$

b) Obs-id: 50093-02-13-01

On the second spectrum, the General model fit the data with a reduced chi-squared of 0.86(42). The Bump and Reflection models also fit the data. The broad gaussian is frozen at 18 keV with a width of 5 keV and the reduced chi-squared is 0.87(41). The scaling factor is stuck to the upper limit of -0.001 and the reduced chi-squared is 0.89(41).

Table 3.9b. Best fitting parameters of the three models and the fluxes. Energies are on keV, fluxes on erg cm^{-2} s^{-1} and normalizations on photons keV^{-1} cm^{-2} s^{-1}. Errors are quoted for 68% confidence level.

Parameters	General model	Bump model	Reflection model
χ^2 (d.o.f)	0.86(42)	0.87(41)	0.89(41)
Γ	$0.18^{+0.07}_{-0.07}$	$0.05^{+0.19}_{-0.16}$	$0.16^{+0.06}_{-0.07}$
E_{cut}	$7.9^{+0.5}_{-0.5}$	$6.8^{+1.5}_{-1.2}$	$7.6^{+0.5}_{-0.6}$
$Normalization_{cutoffpl}$	$0.008^{+0.0005}_{-0.0006}$	$0.007^{+0.001}_{-0.001}$	$0.0081^{+0.0005}_{-0.0005}$
$Flux_{cutoffpl}$	$5.18 \cdot 10^{-10}$	$4.73 \cdot 10^{-10}$	$4.96 \cdot 10^{-10}$
E_{Fe}	6.4	6.4	6.4
EW_{Fe}	$0.09^{+0.3}_{-0.3}$	$0.07^{+0.04}_{-0.04}$	$0.08^{+0.06}_{-0.06}$
σ_{Fe}	0.4	0.4	0.4
$Normalization_{Fe}$	$0.00026^{+0.00009}_{-0.00009}$	$0.0002^{+0.0001}_{-0.0001}$	$0.00021^{+0.00009}_{-0.00008}$
E_{bump}	-	18	-
σ_{bump}	-	5	-
$Normalization_{bump}$	-	$0.0008^{+0.0009}_{-0.0008}$	-
$Rel\text{-}ref_{pexrav}$	-	-	$-0.001^{+0.001}_{-0.002}$
$Flux_{pexrav}$	-	-	$1.38 \cdot 10^{-11}$
Total Flux	$5.20 \cdot 10^{-10}$	$4.98 \cdot 10^{-10}$	$5.15 \cdot 10^{-10}$

c) Obs-id: 50093-02-18-01

On the spectrum with the lowest luminosity, the General model fit the data with a reduced chi-squared of 0.49(42). Both Bump and Reflection models also fit the data. The broad gaussian is at 17.5 keV with a frozen width of 4 keV and the reduced chi-squared is 0.43(40). The iron line was not detected with this model. The scaling factor is stuck to the upper limit of -0.001. The reduced chi-squared for the Reflection model is 0.46(41).

Table 3.9c. Best fitting parameters of the three models and the fluxes. Energies are on keV, fluxes on erg cm^{-2} s^{-1} and normalizations on photons keV^{-1} cm^{-2} s^{-1}. Errors are quoted for 68% confidence level.

Parameters	**General model**	**Bump model**	**Reflection model**
χ^2(d.o.f)	0.49(42)	0.43(40)	0.46(41)
Γ	$0.5^{+0.1}_{-0.1}$	$0.2^{+0.2}_{-0.3}$	$0.8^{+0.1}_{-0.02}$
E_{cut}	$8.3^{+1.5}_{-1.4}$	$5.5^{+1.5}_{-1.2}$	$10.2^{+2.2}_{-2.4}$
$Normalization_{cutoffpl}$	$0.008^{+0.001}_{-0.001}$	$0.006^{+0.001}_{-0.001}$	$0.019^{+0.002}_{-0.002}$
$Flux_{cutoffpl}$	$2.51 \cdot 10^{-10}$	$1.06 \cdot 10^{-10}$	$2.72 \cdot 10^{-10}$
E_{Fe}	6.4	Not detected	6.4
EW_{Fe}	$0.06^{+0.09}_{-0.06}$	-	$0.02^{+0.10}_{-0.02}$
σ_{Fe}	0.4	-	0.4
$Normalization_{Fe}$	$0.00009^{+0.00009}_{-0.00008}$	-	$0.00003^{+0.00009}_{-0.00002}$
E_{bump}	-	$17.5^{+2.8}_{-1.6}$	-
σ_{bump}	-	4	-
$Normalization_{bump}$	-	$0.0009^{+0.0005}_{-0.0005}$	-
$Rel\text{-}ref_{pexrav}$	-	-	$-0.001^{+0.001}_{-0.010}$
$Flux_{pexrav}$	-	-	$3.78 \cdot 10^{-12}$
Total Flux	$2.52 \cdot 10^{-10}$	$2.32 \cdot 10^{-10}$	$2.56 \cdot 10^{-10}$

3.10 XTE J1946+274

The transient Be/X-ray system XTE 1946+274 was first discovered in September of 1998, by the ASM of RXTE (Smith & Tekashima 1998). During 1998 and 2001, the system went through outburst every half orbit (Cambana et al. 1999). The optical counterpart was discovered and identified as a Be star (Verrecchia et al. 2002) and the orbital parameters were determined (Wilson et al. 2003). From RXTE data, a CRSF was found at ~36 keV and the spectrum was described best with the NPEX model (Mihara 1995). After 9 years of quiescence, there was a big outburst in June on 2010 and the same behavior of two outbursts per orbit was observed. This period lasted till June of 2011. After analysis from combined data of RXTE and X-ray Telescope (XRT), the 10 keV feature was detected and fitted as an absorption feature, along with a narrow iron line at 6.4 keV (Muller et al. 2012) and a possible CRSF at ~25 keV. The data from this outburst was best described with a power law with a high energy cut-off.

Spectral fitting

We used the data from the 2010 outburst. We kept the iron line frozen at 6.4 keV, with a 0.1 keV width. On all spectra, the Bump and Reflection models improve the fit significantly. The null hypothesis probabilities are ~0 on all cases.

Table 3.10: The reduced chi-squared for each model and the F-test results: the probabilities for the null hypothesis to be true.

General Model	**Bump Model**		**Reflection model**	
χ^2 (d.o.f)	**F-test: probability**	**χ^2 (d.o.f)**	**F-test probability**	**χ^2 (d.o.f)**
2.96(42)	$4.09 \cdot 10^{-11}$	0.87(39)	$9.94 \cdot 10^{-16}$	0.62(41)
6.24(42)	$1.42 \cdot 10^{-15}$	1.08(39)	$5.91 \cdot 10^{-19}$	0.91(41)
1.63(42)	$3.27 \cdot 10^{-6}$	0.87(39)	$9.53 \cdot 10^{-7}$	0.94(41)

a) Obs-id: 95032-12-01-00

On the spectrum with the highest luminosity, the General model yields a poor fit of a reduced chi-squared of 2.96(42). The Bump and Reflection model both improves the fit with a reduced chi-squared of 0.87(39) and 0.62(41) respectively. The broad gaussian is at 14.4 keV with a 3.7 keV, and the scaling factor is -0.12.

Table 3.10a. Best fitting parameters of the three models and the fluxes. Energies are on keV, fluxes on erg cm^{-2} s^{-1} and normalizations on photons keV^{-1} cm^{-2} s^{-1}. Errors are quoted for 68% confidence level.

Parameters	General model	Bump model	Reflection model
χ^2 (d.o.f)	2.96(42)	0.87(39)	0.62(41)
Γ	$0.41^{+0.02}_{-0.02}$	$0.50^{+0.03}_{-0.04}$	$0.28^{+0.02}_{-0.02}$
E_{cut}	$12.5^{+0.3}_{-0.3}$	$12.0^{+0.8}_{-1.4}$	$7.7^{+0.2}_{-0.2}$
$Normalization_{cutoffpl}$	$0.067^{+0.001}_{-0.001}$	$0.08^{+0.003}_{-0.003}$	$0.063^{+0.001}_{-0.001}$
$Flux_{cutoffpl}$	$5.13 \cdot 10^{-9}$	$4.62 \cdot 10^{-9}$	$3.00 \cdot 10^{-9}$
E_{Fe}	6.4	6.4	6.4
EW_{Fe}	$0.07^{+0.01}_{-0.01}$	$0.08^{+0.01}_{-0.01}$	$0.02^{+0.01}_{-0.01}$
σ_{Fe}	0.1	0.1	0.1
$Normalization_{Fe\text{-}Gauss}$	$0.0014^{+0.0002}_{-0.0002}$	$0.0015^{+0.0003}_{-0.0003}$	$0.0004^{+0.0002}_{-0.0002}$
$E_{10\text{-}bump}$	-	$14.4^{+0.4}_{-0.4}$	-
$\sigma_{10\text{-}bump}$	-	$3.7^{+1.3}_{-0.7}$	-
$Normalization_{10\text{-}bump\text{-}Gauss}$	-	$0.008^{+0.009}_{-0.003}$	-
$Rel\text{-}ref_{pexrav}$	-	-	$-0.12^{+0.01}_{-0.01}$
$Flux_{pexrav}$	-	-	$1.28 \cdot 10^{-9}$
Total Flux	$5.00 \cdot 10^{-9}$	$4.63 \cdot 10^{-9}$	$4.15 \cdot 10^{-9}$

b) Obs-id: 95032-12-04-00

On the second spectrum, the General model does a poor fit of 6.24(42). By adding a broad gaussian at 14.4 keV with a 3.8 keV, the reduced chi-squared goes to 1.08(39). By adding a reflection component with a scaling factor of -0.072, the reduced chi-squared goes to 0.91(41).

Table 3.10b. Best fitting parameters of the three models and the fluxes. Energies are on keV, fluxes on erg cm^{-2} s^{-1} and normalizations on photons keV^{-1} cm^{-2} s^{-1}. Errors are quoted for 68% confidence level.

Parameters	**General model**	**Bump model**	**Reflection model**
χ^2 (d.o.f)	6.24(42)	1.08(39)	0.91(41)
Γ	$0.33^{+0.01}_{-0.01}$	$0.44^{+0.03}_{-0.03}$	$0.22^{+0.01}_{-0.01}$
E_{cut}	$11.8^{+0.2}_{-0.2}$	$11.5^{+0.5}_{-0.7}$	$7.4^{+0.1}_{-0.1}$
$Normalization_{cutoffpl}$	$0.0374^{+0.0005}_{-0.0005}$	$0.047^{+0.001}_{-0.001}$	$0.0363^{+0.0007}_{-0.0006}$
$Flux_{cutoffpl}$	$3.25 \cdot 10^{-9}$	$2.92 \cdot 10^{-9}$	$1.84 \cdot 10^{-9}$
E_{Fe}	6.4	6.4	6.4
EW_{Fe}	$0.074^{+0.006}_{-0.009}$	$0.08^{+0.01}_{-0.01}$	$0.014^{+0.009}_{-0.007}$
σ_{Fe}	0.1	0.1	0.3
$Normalization_{Fe\text{-}Gauss}$	$0.0009^{+0.0001}_{-0.0001}$	$0.0010^{+0.0001}_{-0.0001}$	$0.0002^{+0.0001}_{-0.0001}$
$E_{10\text{-}bump}$	-	$14.4^{+0.3}_{-0.3}$	-
$\sigma_{10\text{-}bump}$	-	$3.8^{+0.7}_{-0.5}$	-
$Normalization_{10\text{-}bump\text{-}Gauss}$	-	$0.006^{+0.003}_{-0.001}$	-
$Rel\text{-}ref_{pexrav}$	-	-	$-0.072^{+0.007}_{-0.007}$
$Flux_{pexrav}$	-	-	$8.61 \cdot 10^{-10}$
Total Flux	$3.19 \cdot 10^{-9}$	$2.94 \cdot 10^{-9}$	$2.65 \cdot 10^{-9}$

c) Obs-id: 95032-12-08-00

On the spectrum with the lowest luminosity, the General model does a fit of 1.63(42). Again, both models improves the fit, giving a reduced chi-squared of 0.87(39) and 0.94(41). The broad gaussian is at 14.8 keV with a 3.6 keV width, and the scaling factor of the reflection component is -0.028.

Table 3.10c. Best fitting parameters of the three models and the fluxes. Energies are on keV, fluxes on erg cm^{-2} s^{-1} and normalizations on photons keV^{-1} cm^{-2} s^{-1}. Errors are quoted for 68% confidence level.

Parameters	**General model**	**Bump model**	**Reflection model**
χ^2 (d.o.f)	1.63(42)	0.87(39)	0.94(41)
Γ	$0.39^{+0.02}_{-0.02}$	$0.4^{+0.1}_{-0.1}$	$0.24^{+0.02}_{-0.02}$
E_{cut}	$11.3^{+0.3}_{-0.3}$	$10.0^{+0.9}_{-1.1}$	$7.60^{+0.3}_{-0.3}$
$Normalization_{cutoffpl}$	$0.0246^{+0.0006}_{-0.0006}$	$0.026^{+0.001}_{-0.001}$	$0.0236^{+0.0005}_{-0.0006}$
$Flux_{cutoffpl}$	$1.69 \cdot 10^{-9}$	$1.50 \cdot 10^{-9}$	$1.12 \cdot 10^{-9}$
E_{Fe}	6.4	6.4	6.4
EW_{Fe}	$0.07^{+0.01}_{-0.01}$	$0.07^{+0.2}_{-0.2}$	$0.03^{+0.01}_{-0.02}$
σ_{Fe}	0.1	0.1	0.1
$Normalization_{Fe\text{-}Gauss}$	$0.00048^{+0.00008}_{-0.00008}$	$0.0005^{+0.0001}_{-0.0001}$	$0.0002^{+0.0001}_{-0.0001}$
$E_{10\text{-}bump}$	-	$14.8^{+0.5}_{-0.7}$	-
$\sigma_{10\text{-}bump}$	-	$3.6^{+6.3}_{-1.1}$	-
$Normalization_{10\text{-}bump\text{-}Gauss}$	-	$0.002^{+0.004}_{-0.001}$	-
$Rel\text{-}ref_{pexrav}$	-	-	$-0.028^{+0.006}_{-0.006}$
$Flux_{pexrav}$	-	-	$3.39 \cdot 10^{-10}$
Total Flux	$1.64 \cdot 10^{-9}$	$1.50 \cdot 10^{-9}$	$1.43 \cdot 10^{-9}$

3.11 V 0332+53

The transient Be/X-ray binary V 0332+53 was detected in 1973 for the first time with the VELA 5B observatory, during a giant outburst (Terrell & Priedhorsky 1984). After 10 years of quiescence, the source went through a series of small outbursts, which was detected with Tenma and EXOSAT satellites, and the orbital parameters were determined (Stella et al. 1995). The position of the optical companion was found (Argyle et al. 1983) and was later identified as a Be star at a distance of ~7 kpc (Nagueruela et al. 1999). The spectrum was fitted with a power law with an exponential cut-off, and showd evidence for a CRSF at ~28 keV. (Makishima et al. 1990). The system underwent a giant outburst in 1989, observed by Ginga (Makino 1989) and two CRSFs were detected at 28.5 and 53 keV (Makishima et al. 1990).The next giant outburst was in 2004. After observations done by the RXTE satellite, three CRSFs were detected at ~27, 51, 74 keV (Coburn et al. 2005). A fluorescent iron line was detected at ~6.4 keV and a power law was used to fit the data (Pottschmidt et al. 2005). There was low X-ray activity in the period of 2008-2010 (Krimm et al. 2008, 2009, Nakajima et al. 2010). The 10 keV feature was detected and fitted as an absorption feature (Caballero et al. 2016). An iron line at 6.4 keV was also present. The source went in to quiescence until June 2015, where a giant outburst occurred.

Spectral fitting

We used the data from the outburst in 2004/2005. The iron line was kept frozen at 6.4 keV with a width of 0.5 keV. In the spectrum with the highest luminosity, both the Bump and Reflection models improved the fit, with the null hypothesis probabilities being ~0 and 0.001 respectively, but since the reduced chi-squared takes such low values (0.5-0.8), it may be that the errors are overestimated. However, on the second spectrum, it's questionable where the fit is improved by the Bump model, since the null hypothesis probability is ~0.1, with a reduced chi-reduced of 0.77, where the General model's is 0.83. The Reflection model does not improve the fit at all. On the lowest luminosity, both models improve the fit, with the null hypothesis probabilities being ~0.

Table 3.11: The reduced chi-squared for each model and the F-test results: the probabilities for the null hypothesis to be true.

General Model	**Bump Model**		**Reflection model**	
χ^2 (d.o.f)	**F-test: probability**	**χ^2 (d.o.f)**	**F-test probability**	**χ^2 (d.o.f)**
1.12(40)	$4.90 \cdot 10^{-7}$	0.52(37)	0.001	0.88(39)
0.83(40)	0.107	0.77(38)	1	0.87(38)
3.44(40)	$2.86 \cdot 10^{-14}$	0.62(37)	$1.03 \cdot 10^{-8}$	1.51(39)

a) Obs-id: 90089-11-05-01

On the first spectrum, all three models fit the data, with the General model having the biggest reduced chi-squared of 1.12(40). The broad gaussian on the case of the Bump model, is at 11.8 keV with a width of 2.4 keV. The scaling factor on the Reflection model, is -0.23. The reduced chi-squared is 0.52(37) and 0.88(39) respectively.

Table 3.11a. Best fitting parameters of the three models and the fluxes. Energies are on keV, fluxes on erg cm^{-2} s^{-1} and normalizations on photons keV^{-1} cm^{-2} s^{-1}. Errors are quoted for 68% confidence level.

Parameters	**General model**	**Bump model**	**Reflection model**
χ^2 (d.o.f)	1.12(40)	0.52(37)	0.88(39)
Γ	$-0.37^{+0.03}_{-0.03}$	$-0.55^{+0.05}_{-0.06}$	$-0.43^{+0.04}_{-0.04}$
E_{cut}	$7.0^{+0.3}_{-0.2}$	$5.5^{+0.4}_{-0.4}$	$6.2^{+0.3}_{-0.3}$
$Normalization_{cutoffpl}$	$0.47^{+0.01}_{-0.01}$	$0.43^{+0.01}_{-0.02}$	$0.45^{+0.01}_{-0.01}$
$Flux_{cutoffpl}$	$9.08 \cdot 10^{-8}$	$7.16 \cdot 10^{-8}$	$7.83 \cdot 10^{-8}$
E_{Fe}	6.4	6.4	6.4
EW_{Fe}	$0.13^{+0.01}_{-0.01}$	$0.126^{+0.01}_{-0.01}$	$0.09^{+0.01}_{-0.01}$
σ_{Fe}	0.5	0.5	0.5
$Normalization_{Fe}$	$0.048^{+0.003}_{-0.003}$	$0.047^{+0.001}_{-0.001}$	$0.034^{+0.006}_{-0.006}$
E_{bump}	-	$11.8^{+0.3}_{-0.4}$	-
σ_{bump}	-	$2.4^{+0.7}_{-0.6}$	-
$Normalization_{bump}$	-	$0.06^{+0.08}_{-0.02}$	-
$Rel\text{-}ref_{pexrav}$	-	-	$-0.23^{+0.07}_{-0.07}$
$Flux_{pexrav}$	-	-	$1.11 \cdot 10^{-8}$
E_{gabs}	30	30	30
σ_{gabs}	$7.1^{+0.1}_{-0.1}$	$6.0^{+0.4}_{-0.6}$	$7.6^{+0.2}_{-0.2}$
Strength	$39.2^{+1.5}_{-1.4}$	$28.1^{+3.3}_{-4.2}$	$38.7^{+1.0}_{-0.9}$
Total Flux	$6.33 \cdot 10^{-8}$	$6.08 \cdot 10^{-8}$	$6.21 \cdot 10^{-8}$

b) Obs-id: 90014-01-04-02

On the second spectra, all three models fit the data. The General model has a reduced chi-squared of 0.83(40). The broad gaussian of the Bump model is at 12.8 keV with a frozen width of 1 keV, and the reduced chi-squared is 0.77(38). The reflection model has a reduced chi-squared of 0.87(38) with the scaling factor being forced to the upper limit of -0.001.

Table 3.11b. Best fitting parameters of the three models and the fluxes. Energies are on keV, fluxes on erg cm^{-2} s^{-1} and normalizations on photons keV^{-1} cm^{-2} s^{-1}. Errors are quoted for 68% confidence level.

Parameters	General model	Bump model	Reflection model
χ^2 (d.o.f)	0.83(40)	0.77(38)	0.87(38)
Γ	$-0.36^{+0.03}_{-0.03}$	$-0.40^{+0.03}_{-0.03}$	$-0.36^{+0.03}_{-0.02}$
E_{cut}	$8.6^{+0.3}_{-0.3}$	$8.0^{+0.3}_{-0.4}$	$8.5^{+0.3}_{-0.6}$
$Normalization_{cutoffpl}$	$0.097^{+0.002}_{-0.002}$	$0.093^{+0.003}_{-0.003}$	$0.097^{+0.002}_{-0.002}$
$Flux_{cutoffpl}$	$2.12 \cdot 10^{-8}$	$2.78 \cdot 10^{-8}$	$2.96 \cdot 10^{-8}$
E_{Fe}	6.4	6.4	6.4
EW_{Fe}	$0.12^{+0.01}_{-0.01}$	$0.11^{+0.01}_{-0.02}$	$0.12^{+0.03}_{-0.03}$
σ_{Fe}	0.5	0.5	0.5
$Normalization_{Fe}$	$0.0111^{+0.0009}_{-0.0009}$	$0.010^{+0.001}_{-0.001}$	$0.011^{+0.002}_{-0.002}$
E_{bump}	-	$12.8^{+0.5}_{-0.5}$	-
σ_{bump}	-	1	-
$Normalization_{bump}$	-	$0.002^{+0.001}_{-0.001}$	-
$Rel\text{-}ref_{pexrav}$	-	-	$-0.001^{+0.001}_{-0.014}$
$Flux_{pexrav}$	-	-	$1.00 \cdot 10^{-10}$
E_{gabs}	30	30	30
σ_{gabs}	$5.7^{+0.1}_{-0.1}$	$5.4^{+0.2}_{-0.2}$	$5.7^{+0.2}_{-0.2}$
Strength	$32.7^{+0.9}_{-0.9}$	$31.8^{+1.0}_{-0.9}$	$32.6^{+0.8}_{-1.4}$
Total Flux	$2.12 \cdot 10^{-8}$	$2.05 \cdot 10^{-8}$	$2.14 \cdot 10^{-8}$

c) Obs-id: 90014-01-07-00

At the lowest luminosity, both the Bump and Reflection models improve the data. The reduced chi-squared is 3.44(40) with the General model and goes to 0.62(37) and 1.51(39) with the Bump and Reflection models respectively. The broad gaussian is at 13.6 keV, with a frozen width of 3 keV, while the scaling factor is at -0.049. The fluorescence iron line was not detected with the reflection model.

Table 3.11c. Best fitting parameters of the three models and the fluxes. Energies are on keV, fluxes on erg cm^{-2} s^{-1} and normalizations on photons keV^{-1} cm^{-2} s^{-1}. Errors are quoted for 68% confidence level.

Parameters	General model	Bump model	Reflection model
χ^2 (d.o.f)	3.44(40)	0.62(37)	1.51(39)
Γ	$0.51^{+0.03}_{-0.03}$	$0.63^{+0.06}_{-0.05}$	$0.27^{+0.03}_{-0.04}$
E_{cut}	$44.4^{+11.5}_{-7.3}$	$24.7^{+8.4}_{-4.0}$	$11.0^{+0.8}_{-0.8}$
$Normalization_{cutoffpl}$	$0.0266^{+0.0008}_{-0.0007}$	$0.040^{+0.002}_{-0.002}$	$0.0234^{+0.0007}_{-0.0008}$
$Flux_{cutoffpl}$	$7.34 \cdot 10^{-9}$	$4.25 \cdot 10^{-9}$	$2.12 \cdot 10^{-9}$
E_{Fe}	6.4	6.4	Not detected
EW_{Fe}	$0.11^{+0.01}_{-0.02}$	$0.046^{+0.02}_{-0.02}$	-
σ_{Fe}	0.5	0.5	-
$Normalization_{Fe}$	$0.0010^{+0.0001}_{-0.0001}$	$0.0004^{+0.0001}_{-0.0001}$	-
E_{bump}	-	$13.6^{+0.3}_{-0.3}$	-
σ_{bump}	-	3	-
$Normalization_{bump}$	-	$0.006^{+0.001}_{-0.001}$	-
$Rel\text{-}ref_{pexrav}$	-	-	$-0.049^{+0.006}_{-0.006}$
$Flux_{pexrav}$	-	-	$1.36 \cdot 10^{-9}$
E_{gabs}	30	30	30
σ_{gabs}	$5.3^{+0.2}_{-0.2}$	$3.5^{+0.6}_{-0.5}$	$5.8^{+0.4}_{-0.4}$
Strength	$36.6^{+2.0}_{-1.9}$	$48.6^{+6.8}_{-6.6}$	$19.7^{+1.5}_{-1.5}$
Total Flux	$7.01 \cdot 10^{-10}$	$6.87 \cdot 10^{-10}$	$7.05 \cdot 10^{-10}$

3.12 4U0115+634

4U 0115+634 is a transient Be/X-ray binary that was first detected in 1969 (Whitlock et al. 1989) during a type II outburst. X-ray pulsations were discovered and the optical companion was identified as a Be star (Cominsky et al. 1978) and it's distance was determined years later, to be ~7 kpc (Negueruela et al. 2001). The orbital parameters were determined (Rappaport et al. 1978) using the SAS data. Coburn (2002) described the spectrum on hard X-rays with a power law with a high energy cut off. He also mentioned the existence of the iron fluorescence line as well as the 10 keV feature. He added a broad gaussian in emission to the model to describe the latter. This source is the only one of which five cyclotron line harmonics have been detected (Muller et al. 2012) at ~10.7, 21.8, 35.5, 46.7, and 59.7 keV. Since it's detection, 4U 0115+634 has been through many type II outbursts, with one happening every 3 to 5 years and lasting for several weeks or months (Jun Li et al. 2012).

Spectral fitting

The data used were taken from the Outburst in 2008. The iron line was kept frozen at 6.4 keV with a width of 0.2 keV. The General model did not fit the data on the first two spectra, with the reduced chi-squared taking values of 4.47(36) and 3.33(36), but on lowest luminosity, it did with a reduced chi-squared of 1.51(36). The Bump model fit the data on all spectra, with the reduced chi-squared taking values between ~0.4-0.8, indicating that the errors may be overestimated. The F-test gives ~0 null hypothesis probabilities for all three spectra. However, the Reflection model turned out to be too simple for a source with multiple cyclotron lines as this one.

Table 3.12: The reduced chi-squared for each model and the F-test results: the probabilities for the null hypothesis to be true.

General Model	**Bump Model**		**Reflection model**	
χ^2 (d.o.f)	**F-test: probability**	**χ^2 (d.o.f)**	**F-test probability**	**χ^2 (d.o.f)**
4.47(36)	$3.89 \cdot 10^{-17}$	0.45(33)	1	4.65(35)
3.33(36)	$5.27 \cdot 10^{-12}$	0.69(33)	1	3.48(35)
1.51(36)	$8.37 \cdot 10^{-5}$	0.87(33)	-	1.59(36)

a) Obs-id: 93032-01-03-00

On the spectrum with the highest luminosity, the General model did not fit the data, giving a reduced chi-squared of 4.47(36) The fit can be improved by using the Bump model: adding a broad gaussian at 10.1 keV with a 2.3 keV width, gives a reduced chi-squared of 0.45 (33). The reflection model did not improve the fit at all, giving a reduced chi-squared of 4.65(35), with a scaling factor that is stuck at the upper limit of -0.001.

Table 3.12a. Best fitting parameters of the three models and the fluxes. Energies are on keV, fluxes on erg cm^{-2} s^{-1} and normalizations on photons keV^{-1} cm^{-2} s^{-1}. Errors are quoted for 68% confidence level.

Parameters	General model	Bump model	Reflection model
χ^2(d.o.f)	4.47(36)	0.45(33)	4.65(35)
Γ	$-0.42^{+0.04}_{-0.04}$	$-0.80^{+0.08}_{-0.09}$	$-0.47^{+0.03}_{-0.05}$
E_{cut}	$11.5^{+1.0}_{-1.0}$	$4.3^{+0.1}_{-0.2}$	$10.14^{+1.5}_{-0.9}$
$Normalization_{cutoffpl}$	$0.109^{+0.003}_{-0.003}$	$0.112^{+0.007}_{-0.008}$	$0.107^{+0.001}_{-0.005}$
$Flux_{cutoffpl}$	$7.85 \cdot 10^{-8}$	$1.80 \cdot 10^{-8}$	$6.69 \cdot 10^{-8}$
E_{Fe}	6.4	6.4	6.4
EW_{Fe}	$0.05^{+0.01}_{-0.01}$	$0.08^{+0.01}_{-0.01}$	$0.045^{+0.01}_{-0.02}$
σ_{Fe}	0.2	0.2	0.2
$Normalization_{Fe}$	$0.006^{+0.001}_{-0.001}$	$0.012^{+0.003}_{-0.002}$	$0.006^{+0.001}_{-0.001}$
E_{bump}	-	$10.1^{+0.2}_{-0.2}$	-
σ_{bump}	-	$2.3^{+0.1}_{-0.1}$	-
$Normalization_{bump}$	-	$0.9^{+0.6}_{-0.2}$	-
$Rel\text{-}ref_{pexrav}$	-	-	$-0.001^{+0.001}_{-0.002}$
$Flux_{pexrav}$	-	-	$2.42 \cdot 10^{-10}$
$E_{gabs,1}$	$12.86^{+0.09}_{-0.08}$	$11.4^{+0.2}_{-0.2}$	$12.82^{+0.09}_{-0.08}$
$\sigma_{gabs,1}$	$2.9^{+0.1}_{-0.1}$	$2.8^{+0.4}_{-0.2}$	$2.8^{+0.1}_{-0.1}$
$Strength_{gabs,1}$	$3.7^{+0.6}_{-0.5}$	$9.1^{+4.4}_{-1.9}$	$3.3^{+0.5}_{-0.5}$
$E_{gabs,2}$	$25.7^{+0.6}_{-0.6}$	$21.7^{+0.8}_{-0.4}$	$25.5^{+0.6}_{-0.6}$
$\sigma_{gabs,2}$	$7.2^{+0.5}_{-0.4}$	$1.39^{+0.6}_{-0.5}$	$7.3^{+0.5}_{-0.4}$
$Strength_{gabs,2}$	$49.5^{+6.9}_{-6.4}$	$0.6^{+1.1}_{-0.3}$	$45.4^{+6.8}_{-6.4}$
Total Flux	$3.46 \cdot 10^{-8}$	$1.75 \cdot 10^{-8}$	$2.96 \cdot 10^{-8}$

b) Obs-id: 93032-01-05-01

On the second spectrum, the General model gives a poor fit of a reduced chi-squared of 3.33(36). The Bump model improves the fit: by adding a broad gaussian at 8.4 keV with a 2.6 keV width, the reduced chi-squared becomes equal to 0.69(33). The reflection model did not improve the fit at all, giving a reduced chi-squared of 3.48(35), with a scaling factor that is stuck at the upper limit of -0.001.

Table 3.12b. Best fitting parameters of the three models and the fluxes. Energies are on keV, fluxes on erg cm^{-2} s^{-1} and normalizations on photons keV^{-1} cm^{-2} s^{-1}. Errors are quoted for 68% confidence level.

Parameters	General model	Bump model	Reflection model
χ^2 (d.o.f)	3.33(36)	0.69(33)	3.48(35)
Γ	$-0.07^{+0.02}_{-0.02}$	$-0.2^{+0.1}_{-0.1}$	$-0.07^{+0.02}_{-0.02}$
E_{cut}	$20.05^{+1.2}_{-1.2}$	$5.6^{+0.6}_{-0.4}$	$19.28^{+1.5}_{-0.9}$
$Normalization_{cutoffpl}$	$0.077^{+0.002}_{-0.002}$	$0.102^{+0.007}_{-0.008}$	$0.076^{+0.001}_{-0.005}$
$Flux_{cutoffpl}$	$5.60 \cdot 10^{-8}$	$7.57 \cdot 10^{-8}$	$5.35 \cdot 10^{-8}$
E_{Fe}	6.4	6.4	6.4
EW_{Fe}	$0.05^{+0.01}_{-0.01}$	$0.06^{+0.01}_{-0.01}$	$0.05^{+0.01}_{-0.01}$
σ_{Fe}	0.2	0.2	0.2
$Normalization_{Fe}$	$0.0030^{+0.0005}_{-0.0005}$	$0.004^{+0.003}_{-0.002}$	$0.0030^{+0.0005}_{-0.0005}$
E_{bump}	-	$8.4^{+0.2}_{-0.1}$	-
σ_{bump}	-	$2.6^{+0.1}_{-0.1}$	-
$Normalization_{bump}$	-	$0.15^{+0.02}_{-0.02}$	-
$Rel\text{-}ref_{pexrav}$	-	-	$-0.001^{+0.001}_{-0.001}$
$Flux_{pexrav}$	-	-	$3.24 \cdot 10^{-10}$
$E_{gabs,1}$	$15.4^{+0.6}_{-0.4}$	$10.4^{+0.2}_{-0.2}$	$15.4^{+0.4}_{-0.4}$
$\sigma_{gabs,1}$	$3.5^{+0.2}_{-0.2}$	$1.8^{+1.0}_{-0.1}$	$3.5^{+0.2}_{-0.2}$
$Strength_{gabs,1}$	$8.9^{+2.7}_{-1.9}$	$0.5^{+0.2}_{-0.5}$	$9.0^{+2.9}_{-2.0}$
$E_{gabs,2}$	$26.3^{+0.4}_{-0.5}$	$21.2^{+0.6}_{-0.3}$	$26.3^{+0.4}_{-0.5}$
$\sigma_{gabs,2}$	$5.3^{+0.4}_{-0.5}$	$1.0^{+0.5}_{-1.0}$	$5.2^{+0.4}_{-0.3}$
$Strength_{gabs,2}$	$60.0^{+7.4}_{-6.2}$	$0.2^{+0.2}_{-0.1}$	$60.9^{+5.2}_{-6.9}$
Total Flux	$3.11 \cdot 10^{-8}$	$9.26 \cdot 10^{-9}$	$2.97 \cdot 10^{-8}$

c) Obs-id: 93032-16-02-01

On the spectrum with the lowest luminosity, the General model fits the data, giving a reduced chi-squared of 1.51(36), which can be improved with the Bump but not with the Reflection model. The Bump model gives a reduced chi-squared of 1.51(36), with the broad gaussian at 9.9 keV with a 2.2 keV width. The Reflection model gives a reduced chi-squared of 1.63(36) with the scaling factor again stuck at -0.001 keV. The iron line was not detectable with the Reflection model.

Table 3.12c. Best fitting parameters of the three models and the fluxes. Energies are on keV, fluxes on erg cm^{-2} s^{-1} and normalizations on photons keV^{-1} cm^{-2} s^{-1}. Errors are quoted for 68% confidence level.

Parameters	General model	Bump model	Reflection model
χ^2 (d.o.f)	1.51(36)	0.87(33)	1.63(36)
Γ	$0.25^{+0.03}_{-0.03}$	$-0.4^{+0.2}_{-0.1}$	$0.22^{+0.02}_{-0.02}$
E_{cut}	$24.74^{+3.2}_{-3.0}$	$4.3^{+0.4}_{-0.1}$	$23.2^{+1.5}_{-0.9}$
$Normalization_{cutoffpl}$	$0.034^{+0.001}_{-0.001}$	$0.029^{+0.004}_{-0.001}$	$0.033^{+0.001}_{-0.005}$
$Flux_{cutoffpl}$	$1.21 \cdot 10^{-8}$	$2.09 \cdot 10^{-8}$	$1.67 \cdot 10^{-8}$
E_{Fe}	6.4	6.4	Not detected
EW_{Fe}	$0.02^{+0.01}_{-0.01}$	$0.06^{+0.01}_{-0.01}$	-
σ_{Fe}	0.2	0.2	-
$Normalization_{Fe}$	$0.0003^{+0.0001}_{-0.0001}$	$0.0009^{+0.0002}_{-0.0002}$	-
E_{bump}	-	$9.9^{+0.2}_{-0.1}$	-
σ_{bump}	-	$2.2^{+0.6}_{-0.2}$	-
$Normalization_{bump}$	-	$0.033^{+0.005}_{-0.009}$	-
$Rel\text{-}ref_{pexrav}$	-	-	$-0.001^{+0.001}_{-0.001}$
$Flux_{pexrav}$	-	-	$1.60 \cdot 10^{-10}$
$E_{gabs,1}$	$16.1^{+0.9}_{-0.7}$	$10.4^{+0.1}_{-0.1}$	$16.3^{+1.1}_{-0.8}$
$\sigma_{gabs,1}$	$3.5^{+0.4}_{-0.3}$	$1.8^{+0.4}_{-0.3}$	$3.6^{+0.3}_{-0.4}$
$Strength_{gabs,1}$	$7.5^{+4.3}_{-2.7}$	$0.5^{+3.2}_{-0.5}$	$8.2^{+5.6}_{-3.8}$
$E_{gabs,2}$	$27.9^{+1.2}_{-0.8}$	$21.2^{+6.0}_{-5.5}$	$27.6^{+0.9}_{-0.6}$
$\sigma_{gabs,2}$	$5.6^{+0.7}_{-0.8}$	$1.0^{+2.4}_{-1.2}$	$5.5^{+0.8}_{-0.9}$
$Strength_{gabs,2}$	$83.9^{+21.0}_{-11.9}$	$0.2^{+27.9}_{-0.2}$	$75.3^{+17.0}_{-8.4}$
Total Flux	$6.52 \cdot 10^{-9}$	$2.32 \cdot 10^{-9}$	$6.37 \cdot 10^{-9}$

Chapter 4: Discussion

We selected twelve transient Be/X-ray binary systems and fit the data from three observations with different luminosities from the PCA instrument of RXTE. For each observations, we used the three different models described on Chapter 2. Our goal was to test if the residuals at 8-12 keV disappear, when an broad gaussian component in emission at 12-18 keV is included, and to provide a physical explanation by testing whether or not the residuals disappear if we use a reflection model on cold material.

On the systems we examined, the 10 keV feature has been previously referenced on 7 out of 12 systems: 4U 1901+03 (Reig et al. 2016), MXB 0656-072 (Nespoli et al. 2012), XTE J1946+274 (Muller et al. 2012), V 0332+52 (Caballero et al. 2016), 4U 0115+634 (Muller et al. 2012), EXO 2030+375 (Epili et al. 2018) and 1A 1118-61 (Suchy et al. 2011). On all of them, the feature was fitted as an absorption feature at 8-12 keV, except from 4U 0115+643, on which it was fitted as emission.

4.1 Bump model

We tried fitting the data with the Bump model, showing that the 10 keV feature disappears when a broad gaussian component in emission is included to the model. We found that in almost every case, an acceptable fit can be obtained, since the residuals on the 8-12 keV energy range completely disappear. More precisely, on every system, except for XTE J1543-568, the F-test gave zero null hypothesis probabilities (smaller than 10^{-6}), that is the improvement in the fit by the the addition of a broad gaussian at the 12-18 energy range with a width of 3-6 keV to occur by change. Therefore, the component is statistically significant.

A correlation between the iron line's normalization and the flux of the model exists, with a Pearson correlation coefficient of 0.9, indicating that the Iron line's existence is due to reflection.

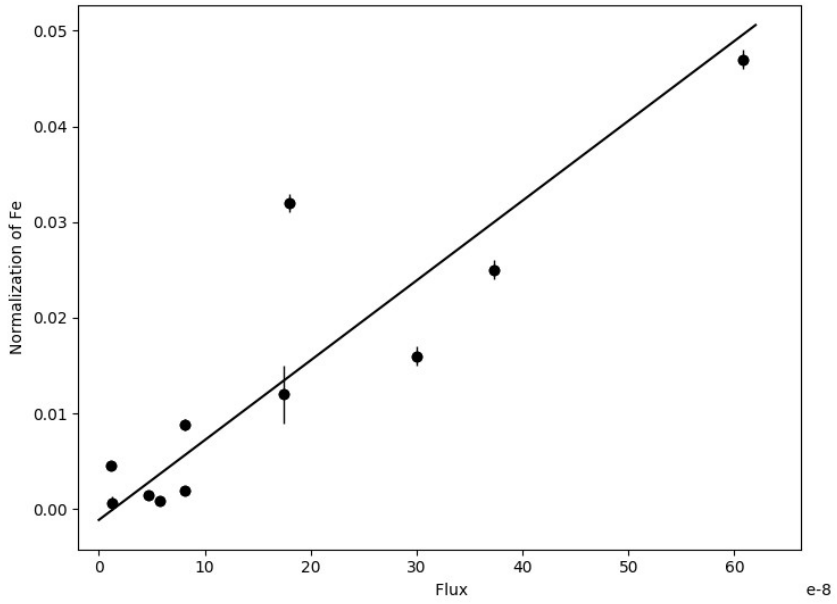

Figure 4.1: Normalization of the Iron's gaussian (keV^{-1} cm^{-2} s^{-1}) vs. Flux (10^{-8} erg cm^{-2} s^{-1}) . It does not include A0535+26. We used the highest luminosity spectra, since they have a better S/N ratio.

Since the iron line is originated from reflection and is present on every fit, along with the fact that the broad emission component provide such good fit on the data set, raises the question whether or not the broad emission originates from reflection as well.

4.2 Reflection model

The pexrav model that was used as the reflection component has two problems: it is not referring to Be/X-ray binaries but to Black Hole X-ray binaries (BHXBs) (A.C. Fabian and R.R. Ross et al. 2010), and it's simplistic, meaning that there are several approximations made (semi-infinite, plane parallel and completely neutral material) (Magdziarz & Zdziarski 1995). Nonetheless, the fit in most cases was better with the reflection model, than with the simple general model on the spectra with the highest luminosities, but there was moderate success on the lower ones. We should note that the model had no success on fitting a system with multiple cyclotron features, like the system 4U 0115+633

There are some indications that may favor the possibility for the broad emission at the energy range of 12-18 keV to originate from reflection. Aside from the fact that the model did improve the fit in many cases, there is a correlation between the normalization of the gaussian used to fit the iron line and the scaling factor, with a Pearson correlation coefficient of -0.8. This result is referring only for the spectra with the highest luminosity for each system, since the S/N ratio is better. Finally, when the Reflection model does fit the data, the Bump model does as well.

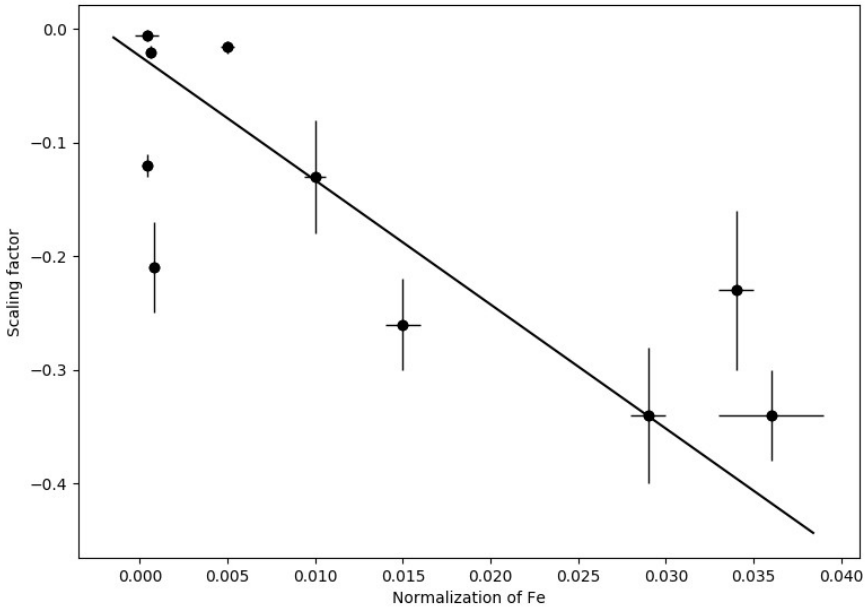

Figure 4.2: Scaling factor vs. Normalization of Fe (keV^{-1} cm^{-2} s^{-1}) for the highest luminosities. EXO 2030+375 (Unreasonable high value of -5.8) and 4U0115+634 are excluded.

4.3 Conclusion

The residuals at 8-12 keV appear when the typical phenomenological model for accreting pulsar, a power law with a high energy cutoff, is used to fit the data of transient Be/X-ray binaries. In previous works, a Gaussian profile was used to fit the residuals, either in emission or absorption, but no physical explanation has been given about the origin of the residuals. The fact that the 10 keV feature appears in the spectra of BeXBs that both exhibit or do not exhibit cyclotron lines, follows to the conclusion that it is not a magnetic feature.

As for the possibility of the 10 keV feature to be of instrumental origin, Rothschild et al. (2006) assumed that it might be due to the copper fluorescence line from the collimator of the PCA instrument of RXTE. They included a narrow Gaussian component in emission, at 8.04 keV, which is the K_α fluorescence line of copper. Doroshenko et al. (2010), while studying 1A 1118-61, also found residuals at ~8 keV. They also included a frozen narrow Gaussian in emission, at 8.04 keV. They referenced Coburn's (2002) phenomenological model for fitting the 10 keV feature, indicating that it's the same feature. Until Doroshenko's publication on 2010, the feature had been detected with three satellites: RXTE, Ginga and BeppoSAX. The collimators on all of them contains copper and a logical assumption would be to that the 10 keV feature is of systematic origin after all. Suchy et al. (2011) detected the feature with Suzaku, which doesn't have any copper. They used a broad Gaussian in absorption at ~10 keV to describe it.

In our work, we used three different models, the typical phenomenological model for accreting pulsars, a phenomenological model that includes a broad Gaussian in emission and a physical model that includes reflection from cold material in the vicinity of the compact object. The typical phenomenological model always left residuals at 8-12 keV, when the S/N ratio was good. When the broad Gaussian at 12-18 keV was added to the model, the residuals were mostly gone. The Reflection model had good results when the S/N was good in most of the spectra. However, when the source exhibit multiple cyclotron lines (4U 0115+634), the Reflection model did not fit the data at all.

The question is whether the 10 keV feature is real and has a physical origin or if the power law with a high energy cutoff is too simple as a phenomenological model to describe the spectra of transient Be/X-ray binaries. If it's real, then reflection might be the origin, since we got moderate to good results with such a simple model. A more complex reflection model is required to test this hypothesis. There is always the possibility that the 10 keV feature is of instrumental origin but more research is needed.

References

1. A. Manousakis, V. Beckmann , V. Bianchin , S. Brandt, J. Chenevez , W. Hermsen, A. von Kienlin , R. Krivonos , M. Mas-Hesse: INTEGRAL hard X-ray detection of HMXB GX 304-1 and H 1417-624. (2018)

2. Apparao, K.M.V.; Naraman, S. . & Kelley, R.L.; Bradt, H.V.; Massachusetts Inst. of Tech., C. 2S 1417-624: A Variable Galactic X-ray Source Near CG312-1. (1980)

3. Argyle, R. W.; Kodaira, K.; Bernacca, P. L.; Iijima, T.; Stagni, R. V0332+53. (1983)

4. Ballhausen, R. et al. Looking at A 0535+26 at low luminosities with NuSTAR. Astron. Astrophys. 608, 1–14 (2017).

5. Balucinska-Church, Monika; McCammon, D. Photoelectric Absorption Cross Sections with Variable Abundances. (1992)

6. Borozdin, K.; Gilfanov, M.; Sunyaev, R.; Churazov, E.; Loznikov, V.; Yamburenko, N.; Skinner, G. K.; Patterson, T. G.; Willmore, A. P.; Emam, O.; Brinkman, A. C.; Heise, J.; Int-Zand, J. J. M.; Jager, R. KS:1947+300 - a new transient X-ray source in Cygnus. (1990)

7. Brown, A. G. A. et al. Gaia Data Release 1: Summary of the astrometric, photometric, and survey properties. Astron. Astrophys. 595 (2016).

8. Caballero-García, M. D. et al. Activity from the Be/X-ray binary system V0332+53 during its intermediate-luminosity outburst in 2008. Astron. Astrophys. 589 (2016).

9. Caballero, I. et al. Peculiar outburst of A0535+26 observed with INTEGRAL, RXTE and suzaku. Proc. Sci. (2009)

10. Caballero, I. et al. A double-peaked outburst of A 0535+26 observed with INTEGRAL, RXTE, and Suzaku. Astrophys. J. Lett. 764, 1–5 (2013).

11. Campana, S., Israel, G. & Stella, L. Evidence for an ∼ 80 day periodicity in the X-ray transient pulsar XTE J1946+274. Astron. Astrophys. 352, 1–4 (1999).

12. Chevalier, C.; Ilovaisky, S. A. X-ray sources. (1975)

13. Clark, G. W.; Schmidt, G. D.; Angel, J. R. P. MX0656-07. (1975)

14. Coburn, W. et al. Magnetic Fields of Accreting X-Ray Pulsars with the Rossi X-Ray Timing Explorer . Astrophys. J. 580, 394–412 (2002).

15. Coburn, W.; Kretschmar, P.; Kreykenbohm, I.; McBride, V. A.; Rothschild, R. E.; Wilms, J. Multiple Cyclotron Lines in V0332+53.

16. Coe, M. J. & Laycock, S. A decade in the life of EXO 2030+375:A multiwavelength study of an accreting X-ray pulsar; Colleen A. Wilson 1 and Mark H. Finger 2. 287–302 (2002).

17. Cominsky, L.; Li, F.; Bradt, H.; Clark, G. W.; Rappaport, S.; Johnston, M.; Doxsey, R.; Gursky, H.; Schwartz, D.; Schwarz, J. 4U 0115+63. (1978)

18. Devasia, J., James, M., Paul, B. & Indulekha, K. RXTE-PCA observations of 1A 1118-61: Timing and spectral studies during an outburst. Mon. Not. R. Astron. Soc. 414, 1023–1031 (2011).

19. Doroshenko, V. et al. RXTE observations of the 1A 1118-61 in an outburst, and the discovery of a cyclotron line. Astron. Astrophys. 515, 20–23 (2010).

20. Epili, P., Naik, S., Jaisawal, G. K. & Gupta, S. Decade long RXTE monitoring observations of Be/X-ray binary pulsar EXO 2030+375. Mon. Not. R. Astron. Soc. 472, 3455–3466 (2017).

21. Eyles, C. J.; Skinner, G. K.; Willmore, A. P.; Rosenberg, F. D. Variable X-ray source near Cen X-3. (1975)

22. Fabian, A. C. & Ross, R. R. X-ray reflection. Space Sci. Rev. 157, 167–176 (2010).

23. Farinelli, R., Ferrigno, C., Bozzo, E. & Becker, P. A. A new model for the X-ray continuum of the magnetized accreting pulsars. Astron. Astrophys. 591, (2016).

24. Ferrigno, C. et al. A constant Cyclotron Line Energy in 4U 0115+634. (2012).

25. Finger, M. H., Wilson, R. B., & Chakrabarty, D. Reappearance of the X-ray binary pulsar 2S 1417-624. (1395).

26. Finger, M. H.; Wilson, R. B.; Harmon, B. A. Quasi-periodic Oscillations during a Giant Outburst of A0535+262. (1395).

27. Forman, W.; Jones, C.; Tananbaum, H. Survey of intensity variability of strong galactic X-ray sources from Uhuru. (1976)

28. Galloway, D. K., Morgan, E. H. & Levine, A. M. A Frequency Glitch in an Accreting Pulsar. Astrophys. J. 613, 1164–1172 (2004).

29. Galloway, D.; Remillard, R.; Morgan, E.; Swank, J. X1901+031. (2003)

30. Galloway, D. K., Wang, Z. & Morgan, E. H. Discovery of Pulsations in the X-Ray Transient 4U 1901+03. Astrophys. J. 635, 1217–1223 (2005).

31. Grindlay, J. E., Band, D., Seward, F., Leahy, D., Weisskopf, M. C., & Marshall, F. E. The central X-ray source in SS 433. (2000)

32. Grudzinska, M. et al. On the formation and evolution of the first Be star in a black hole binary MWC 656. Mon. Not. R. Astron. Soc. 452, 2773–2787 (2015).

33. Hattori, S., Ota, N., Zhang, Y.-Y., Akamatsu, H. & Finoguenov, A. arXiv:1702.02157v1 [astro-ph.HE] 7 Feb 2017. Publ. Astron. Soc. Japan 00, 1–9 (2014).

34. Hayasaki, K. & Okazaki, A. T. Accretion disc formation around the neutron star in Be/X-ray binaries. Mon. Not. R. Astron. Soc. 350, 971–982 (2004).

35. Ilovaisky, S. A.; Chevalier, C. Rapid spectroscopic changes in HZ herculis. (1974)

36. in ’t Zand, J. J. M., Corbet, R. H. D. & Marshall, F. E. Discovery of a 75 Day Orbit in XTE J1543−568. Astrophys. J. 553, L165–L168 (2001).

37. Jaisawal, G. K., Naik, S. & Epili, P. Suzaku view of the Be/X-ray binary pulsar GX 304-1 during Type I X-ray outbursts. Mon. Not. R. Astron. Soc. 457, 2749–2760 (2016).

38. James, M., Pau, B., Devasia, J. & Indulekha, K. Flares, broadening of the pulse-frequency peak and quasi-periodic oscillations in the transient X-ray pulsar 4U 1901+03. Mon. Not. R. Astron. Soc. 410, 1489–1495 (2011).

39. K. Pottschmidt ,V. A. McBride, S. Suchy, I. Kreykenbohm , J. Wilms , R. E. Rothschild, P. Kretschmar, G. Schoe, J. H. S. : RXTE observations of MXB 0656-072. (2007)

40. Kennea, J. A.; Romano, P.; Pottschmidt, K.; Wilms, J.; Cummings, J.; Evans, P.; Burrows, D. N. Swift and RXTE observations of MXB 0656-072. (2007)

41. Kretschmar, P.; Pan, H. C.; Kendziorra, E.; Kunz, M.; Maisack, M.; Staubert, R.; Pietsch, W.; Truemper, J.; Efremov, V.; Sunyaev, R. Absorption features in the hard X-ray spectra of PSR A 0535+26 and Vela X-1. (1996)

42. Kreykenbohm, I.; Shaw, S. E.; Bianchin, Valentina; Diehl, R.; Brandt, S.; Mas-Hesse, M.; Parmar, A.; Hermsen, W.; Krivonos, R. INTEGRAL detects a new outburst of MXB 0656-072. (2007)

43. Krimm, H. A.; Barthelmy, S. D.; Baumgartner, W.; Cummings, J. R.; Fenimore, E.; Gehrels, N.; Markwardt, C. B.; Palmer, D.; Parsons, A. M.; Sakamoto, T.; Skinner, G.; Stamatikos, M.; Tueller, J. Swift/BAT detects renewed activity from V0332+53. (2008)

44. Krimm, H. A.; Barthelmy, S. D.; Baumgartner, W.; Cummings, J.; Fenimore, E.; Gehrels, N.; Markwardt, C. B.; Palmer, D.; Sakamoto, T.; Skinner, G.; Stamatikos, M.; Tueller, J.; Ukwatta, T. Swift reports a recent brightening of XTE J1543-568. (2012)

45. Krimm, H. A.; Barthelmy, S. D.; Baumgartner, W.; Cummings, J.; Fenimore, E.; Gehrels, N.; Markwardt, C. B.; Palmer, D.; Sakamoto, T.; Skinner, G.; Stamatikos, M.; Tueller, J.; Ukwatta, T. Swift/BAT detects renewed activity from V0332+53. (2009)

46. Krimm, H.; Barthelmy, S.; Gehrels, N.; Markwardt, C.; Palmer, D.; Sanwal, D.; Tueller, J. Swift/BAT detects an outburst from EXO 2030+375. (2013)

47. Lei, Y. J. et al. Phase-resolved spectral analysis of 4U 1901+03 during its outburst. Astrophys. J. 707, 1016–1022 (2009).

48. Levine, A. M. et al. First Results from the All-Sky Monitor on the [ITAL]Rossi X-Ray Timing Explorer[/ITAL]. Astrophys. J. 469, L33–L36 (1996).

49. Li, F.; Rappaport, S.; Clark, G. W.; Jernigan, J. G. A0535+26: a refined position measurement and new pulse period data. (1979)

50. Lin, L. C. C., Takata, J., Kong, A. K. H. & Hwang, C. Y. Swift observations of the Be/X-ray transient system 1A 1118-615. Mon. Not. R. Astron. Soc. 409, 1127–1135 (2010).

51. M. J. Coe, A. Longmore, B. J. Payne, C. G. H. The optical/IR counterpart to the newly-discovered X-ray source EXO 2030+375. (1998)

52. Magdziarz, Pawel; Zdziarski, A. A. Angle-dependent Compton reflection of X-rays and gamma-rays. (1995)

53. Maisack, M. et al. Pulse phase spectroscopy of A 0535+26 during its 1994 giant outburst observed with OSSE. Astron. Astrophys. 325, 212–216 (1997).

54. Makino, F. . G. T. X0331+53. (1989)

55. Makishima, Kazuo; Ohashi, Takaya; Kawai, Nobuyuki; Matsuoka, Masaru; Koyama, Katsuji; Kunieda, Hideyo; Tawara, Yuzuru; Ushimaru, Naoko; Corbet, Robin H. D.; Inoue, Hajime; Kii, Tsuneo; Makino, Fumiyoshi; Mitsuda, Kazuhisa; Murakami, Toshio; Nagase, Fumiak, K. Observations of the Peculiar Hard X-Ray Transient X0331+53 (V0332+53).

56. Mark T. Stollberg, Mark H. Finger, Robert B. Wilson, D. Matthew Scott, David J. Crary, and W. S. P. Orbit determination for the Be/X-ray transient EXO 2030+375. (1999)

57. Marshall, F. E.; Takeshima, T.; in ’t Zand, J. XTE J1543-568. (2000)

58. McBride, V. A. et al. Study of the cyclotron feature in MXB 0656-072. Astron. Astrophys. 451, 267–272 (2006).

59. McClintock, J. E.; Rappaport, S. A.; Nugent, J. J.; Li, F. K. Discovery of a 272 second periodic variation in the X-ray source GX 304-1. (1971)

60. Mihara. Observational Study of X-ray spectra of Binary Pulsars with Ginga. (1995).

61. Molkov, S., Lutovinov, A. & Grebenev, S. First results from TOO observations of the Aql X-1 field with INTEGRAL. Astron. Astrophys. 411, (2003).

62. Motch, C.; Janot-Pacheco, E. The optical counterpart of the X-ray transient EXO 2030+375.

63. Müller, D., Klochkov, D., Caballero, I. & Santangelo, A. Astrophysics A 0535 + 26 in the April 2010 outburst : probing the accretion. 81, 1–9 (2013).

64. Müller, S. et al. The reawakening of the sleeping X-ray pulsar XTE J1946+274. Astron. Astrophys. 546, 1–9 (2012).

65. Negueruela, I., Israel, G. L., Marco, A., Norton, A. J. & Speziali, R. The Be/X-ray transient KS 1947+300. Astron. Astrophys. 397, 739–745 (2003).

66. Negueruela, I. & Okazaki, A. T. The Be/X-ray transient 4U 0115+63/V635 Cassiopeiae. I. A consistent model. Astron. Astrophys. 369, 108–116 (2001).

67. Negueruela, I., Roche, P., Fabregat, J. & Coe, M. J. The Be/X-ray transient V0332+53: Evidence for a tilt between the orbit and the equatorial plane? Mon. Not. R. Astron. Soc. 307, 695–702 (1999).

68. Nespoli, E., Reig, P. & Zezas, A. New insights into the Be/X-ray binary system MXB 0656-072. Astron. Astrophys. 547, 1–8 (2012).

69. Oliver, J. A photometric and spectroscopic study of He 3-640 (?=A 1118-61). J. Chem. Inf. Model. 53, 1689–1699 (2013).

70. Pakull, Manfred W.; Motch, Christian; Negueruela, I. Be star counterpart of X-ray pulsar MX0656-072.(2003)

71. Parkes, G. E.; Murdin, P. G.; Mason, K. O. The shell spectrum of the optical counterpart of GX 304-1 (4U 1258-61). (1980)

72. Paul, B. & Naik, S. Transient high mass x-ray binaries. Bull. Astron. Soc. India 39, 429–449 (2011).

73. Peter Jenke (MSFC/NPP), M. H. F. (USRA). 4U 1901+03 observations with Fermi/GBM.
74. Rappaport, S.; Clark, G. W.; Cominsky, L.; Joss, P. C.; Li, F. Orbital elements of 4U 0115+63 and the nature of the hard X-ray transients. 32, 147–156 (1978).

75. Reig, P. & Coe, M. J. Timing properties of the X-ray pulsar EXO 2030 + 375 during an X-ray outburst. Mon. Not. R. Astron. Soc. 294, 118–126 (1998).

76. Reig, P. & Milonaki, F. Accretion regimes in the X-ray pulsar 4U 1901+03. Astron. Astrophys. 594, 1–10 (2016).

77. Reig, P. Be/X-ray binaries. Astrophys. Space Sci. 332, 1–29 (2011).

78. Rivinius, T., Carciofi, A. C. & Martayan, C. Classical Be stars: Rapidly rotating B stars with viscous Keplerian decretion disks. Astron. Astrophys. Rev. 21, (2013).

79. Rodes-Roca, J. J. et al. The first cyclotron harmonic of 4U 1538-52. Astron. Astrophys. 508, 395–400 (2009).

80. Rothschild, R. E. et al. INTEGRAL and RXTE Observations of Centaurus A . Astrophys. J. 641, 801–821 (2006).

81. S. Müller, C. Ferrignob, M. Kühnela, G. Schönherrc, P. A. Beckerd, M. T. Wolffe, D. Hertela, F.-W. Schwarma, V. Grinberga, M. Obsta, I. Caballerof, K. Pottschmidtg, F. Fürsth, I. Kreykenbohma, R. E. Rothschildi, P. Hemphilli, S. Martínez Núñezj, J. M. Tor, R. S. and J. W. A constant Cyclotron Line Energy in 4U 0115+634 S. (2012).

82. Santangelo, A. et al. Beppo SAX detection of a Cyclotron Feature in the spectrum of Cen X-3. Astron. Astrophys. 340, (1998).

83. Smith, D. A.; Takeshima, T. XTE J1946+274 Transient 15.8-s Pulsar (= 3A 1942+274 ?). (1998)

84. Staubert, R. et al. Cyclotron lines in highly magnetized neutron stars. Astron. Astrophys. 622, (2019).

85. Steele, I. A., Negueruela, I., Coe, M. J. & Roche, P. The distances to the X-ray binaries LSI +61° 303 and A0535+262. Mon. Not. R. Astron. Soc. 297, (1998).

86. Stella, L.; White, N. E.; Davelaar, J.; Parmar, A. N.; Blissett, R. J.; van der Klis, M. The discovery of 4.4 second X-ray pulsations from the rapidly variable X-ray transient V 0332+53. (1995)

87. Stella, L., White, N. E. & Rosner, R. Intermittent stellar wind accretion and the long-term activity of Population I binary systems containing an X-ray pulsar. Astrophys. J. 308, 669 (1986).

88. Suchy, S. et al. Suzaku observations of the HMXB 1A1118-61. Astrophys. J. 733, (2011).

89. Suchy, S. et al. Pulse Phase-Resolved Analysis of the High-Mass X-Ray Binary Centaurus X-3 over Two Binary Orbits. Astrophys. J. 675, 1487–1498 (2008).

90. T. Yamamoto (RIKEN), M. Nakajima (Nihon U), T. Mihara, M. Sugizaki, M. Serino, S. Nakahira, T. Sootome, M. Matsuoka (RIKEN), S. Ueno, H. Tomida, M. Kohama, M. Ishikawa (JAXA), N. Kawai, M. Morii, K. Sugimori, R. Usui, T. Toizumi (Tokyo Tech), A. Yoshida, K. Y. (Chuo U. . report on behalf of the M. team. MAXI/GSC detection of a brightening of X-ray binary pulsar 4U 0115+63.

91. Terrell, J.; Priedhorsky, W. C. The 1973 X-ray transient V 0332+53. (1395).

92. Torrejón, J. M., Schulz, N. S., Nowak, M. A. & Kallman, T. R. A Chandra survey of fluorescence Fe lines in X-ray binaries at high resolution. Astrophys. J. 715, 947–958 (2010).

93. Tsygankov, S. S. & Lutovinov, A. A. Observations of the Transient X-ray Pulsar KS 1947+300 by the INTEGRAL and RXTE Observatories. Astron. Lett. 31, 380–387 (2005).

94. Vasco, D. et al. Pulse phase and precession phase resolved spectroscopy of Hercules X-1: Studying a representative Main-On with RXTE. Astron. Astrophys. 550, 1–10 (2013).

95. Verrecchia, F. et al. Astrophysics The identification of the optical / IR counterpart of the 15 . 8-s transient X – ray pulsar XTE J1946 + 274. 989, 983–989 (2002).

96. White, N. E.; Swank, J. H.; Holt, S. S. Accretion powered X-ray pulsars. (1983)

97. Whitlock, L., Roussel-Dupre, D., & Priedhorsky, W. Observations of the X-ray transient 4U 0115+63. J. Japan Soc. Air Pollut. 24, 45–51 (1989).

98. Wilson, C. A., Finger, M. H. & Camero-Arranz, A. Outbursts Large and Small from EXO 2030+375. Astrophys. J. 678, 1263–1272 (2008).

99. Wilson, C. A., Finger, M. H., Coe, M. J. & Negueruela, I. XTE J1946+274 = GRO J1944+26: An Enigmatic Be/X-ray Binary. (2002)

100. Yamamoto, T.; Nakahira, S.; Kawai, N.; Negoro, H.; Makishima, K.; Sugizaki, M.; Nakajima, M.; Sugimori, K.; Matsuoka, M. MAXI/GSC detection of an outburst from GX 304-1. (2009)

101. Yamamoto, T. et al. Discovery of a Cyclotron Resonance Feature in the X-Ray Spectrum of GX 304−1 with RXTE and Suzaku during Outbursts Detected by MAXI in 2010. Publ. Astron. Soc. Japan 63, S751–S757 (2011).

102. Yan, J. et al. Multi-wavelength study of the Be/X-ray binarya MXB 0656 − 072. (2012).

103. Biswajit Paul and Sachindra Naik: Transient High Mass X-ray Binaries , BASI, 39, 429 (2011).

104. *https://heasarc.gsfc.nasa.gov/docs/xte/appendix_f.html*

105. *https://heasarc.gsfc.nasa.gov/xanadu/xspec/manual/XspecManual.html*